MSDE

Molecular Systems Design & Engineering

Accepted Manuscript

This article can be cited before page numbers have been issued, to do this please use: D. Danaci, M. Bui, N. Mac Dowell and C. Petit, *Mol. Syst. Des. Eng.*, 2019, DOI: 10.1039/C9ME00102F.

ROYAL SOCIETY OF CHEMISTRY

rsc.li/molecular-engineering

View Article Online
DOI: 10.1039/C9ME00102F

Exploring the limits of adsorption-based CO_2 capture using MOFs with PVSA – from molecular design to process economics

David Danaci[a,b], *Mai Bui*[c,d], *Niall Mac Dowell*[c,d,*], *Camille Petit*[a,b,*]

a – Department of Chemical Engineering, Imperial College London, South Kensington, London, SW7 2AZ, UK

b – Barrer Centre, Imperial College London, South Kensington, London, SW7 2AZ, UK

c – Centre for Environmental Policy, Imperial College London, South Kensington, London, SW7 1NE, UK

d – Centre for Process Systems Engineering, Imperial College London, South Kensington, London, SW7 2AZ, UK

DESIGN, SYSTEM, APPLICATION

Adsorption-based processes represent one of the proposed routes for post combustion CO_2 capture. The design and operation of an adsorption process, and

subsequently its feasibility, centres around the adsorbent, *i.e.* the porous material used to carry out the separation between CO_2 and N_2 molecules. As such, evaluating adsorbents and identifying adsorbent properties that yield both technically and economically feasible designs is paramount to test the potential of adsorption-based carbon capture at large scale. This task is particularly important given the thousands of adsorbents that exist.

Adsorption processes are inherently highly coupled systems. For example, an adsorbent with a very high capacity will have a correspondingly high temperature change upon adsorption, which will reduce the equilibrium loading of that sorbent. The total energy released upon adsorption is the product of amount adsorbed and enthalpy of adsorption. Thus, an optimum would exist for capacity which will balance this trade-off.

Our work relates adsorbent properties with process performance both from a technical, and economic perspective. Including the link between molecular-level material properties and process cost expedites the design of new fit-for-purpose adsorbents. This work can be used to guide, or change the focus of, future adsorbent development for post-combustion capture applications.

View Article Online
DOI: 10.1039/C9ME00102F

Exploring the limits of adsorption-based CO_2 capture using MOFs with PVSA – from molecular design to process economics

David Danaci[a,b], Mai Bui[c,d], Niall Mac Dowell[c,d,], Camille Petit[a,b,*]*

a – Department of Chemical Engineering, Imperial College London, South Kensington, London, SW7 2AZ, UK

b – Barrer Centre, Imperial College London, South Kensington, London, SW7 2AZ, UK

c – Centre for Environmental Policy, Imperial College London, South Kensington, London, SW7 1NE, UK

d – Centre for Process Systems Engineering, Imperial College London, South Kensington, London, SW7 2AZ, UK

KEYWORDS: MOF, post combustion CO_2 capture, adsorption, cost, PSA model, screening tool, amine absorption

ABSTRACT

View Article Online
DOI: 10.1039/C9ME00102F

Metal-organic frameworks (MOFs) have taken the materials science world by storm, with potentials of near infinite possibilities and the panacea for adsorption-based carbon capture. Yet, no pilot-scale (or larger-scale) study exists on MOFs for carbon capture. Beyond material scalability issues, this clear gap between the scientific and engineering literature relates to the absence of suitable and accessible assessment of MOFs in an adsorption process.

Here, we have developed a simple adsorbent screening tool with process economics to evaluate adsorbents for post-combustion capture, while also considering factors relevant to industry. Specifically, we have assessed the 25 adsorbents (22 MOFs, 2 zeolites, 1 activated carbon) against performance constraints – *i.e.* CO_2 purity and recovery – and cost. We have considered four different CO_2 capture scenarios to represent a range of CO_2 inlet concentrations. The cost is compared to that of amine-based solvents for which a corresponding model was developed. Using the model developed, we have conceptually assessed the materials properties and process parameters influencing the purity, recovery and cost in order to design the 'best' adsorbent. We have also set-up a tool for readers to screen their own adsorbent.

In this contribution, we show that minimal N_2 adsorption and moderate enthalpies of adsorption are key in obtaining good process performance and reducing cost. This stands in contrast to the popular approaches of maximizing CO_2 capacity or surface area. Of the 22 MOFs evaluated, UTSA-16 shows the best performance and lowest cost for post-combustion capture, having performance in-line with the benchmark, zeolite 13X. Mg-MOF-74 performs poorly. The cost of using the adsorbents remains overall higher than that of an amine-based absorption process.

Ultimately, this study provides specific directions for material scientists to design adsorbents and assess their performance at the process scale. This works intends to bridge the gap between scientific

and engineering studies to accelerate CO_2 capture adsorbents development. The approach can be extended to other molecular separations.

View Article Online
DOI: 10.1039/C9ME00102F

INTRODUCTION

Despite nearly two decades of intense research effort, some could argue that the field of so-called "designer adsorbents" is still more of a scientific curiosity than a fully realised tool. Designer adsorbents allow one to tune materials for a given application, *e.g.* CO_2 capture in the context of the present study. Heavily researched exemplars of designer adsorbents are metal organic frameworks (MOFs). A number of MOFs have been tested at lab-scale[1–19]. These studies typically place a large emphasis on unveiling the molecular separation mechanisms and enhancing CO_2 uptake, selectivity (*e.g.* ideal selectivity (Eq 1), or Henry selectivity (Eq 2)), or working capacity (Eq 3).

$$S_{A/B}^{ideal} = \frac{n_A\left(P_A^{feed}, T^{feed}\right)\cdot y_B^{feed}}{n_B\left(P_B^{feed}, T^{feed}\right)\cdot y_A^{feed}} \quad (1)$$

Where n_j is the uptake of component j at the partial pressure of j in the feed (P_j^{feed}) at the feed temperature T^{feed}, and y_j^{feed} is the molar fraction of j in the feed gas.

$$S_{A/B}^{Henry} = \frac{H_A\left(T^{feed}\right)}{H_B\left(T^{feed}\right)} \quad (2)$$

Where H_j is the Henry constant for component j at the feed temperature, T^{feed}.

$$WC_A^{pure} = n_A\left(P^{feed}\cdot y_A^{feed}, T^{feed}\right) - n_A\left(P^{des}\cdot y_A^{feed}, T^{feed}\right) \quad (3)$$

Where $n_A(P,T)$ is the uptake of component A at a partial pressure P and temperature T, P^{feed} and P^{des} are the feed and desorption pressures respectively, T^{feed} is the feed temperature, and y_A^{feed} is the molar fraction of A in the feed gas.

While these are necessary features to investigate, they are in no way sufficient. For instance, an adsorbent should also exhibit a "fast" rate of mass transfer (non-limiting) and be "easily" regenerated under moderate conditions.

View Article Online
DOI: 10.1039/C9ME00102F

Comparatively to the number of lab scale research studies, progress towards scale-up remains very slow. Hence, it becomes clear that in order to transition to the next stage or technology readiness level (TRL), one cannot rely solely on the current practice of *post-hoc* rationalisation of materials to maximise CO_2 uptake, CO_2/N_2 selectivity or working capacity. Such an approach makes it impossible to reliably and quickly determine the most promising materials (and material attributes), especially when those are highly tuneable as in MOFs. To address this knowledge gap, links must be drawn between the adsorbent design and the adsorption process. In other words, adsorbent properties should be screened/evaluated using a process performance index. The screening tool should provide a framework based on selected metrics that define a range of acceptable values for each of the process parameters considered. Typical parameters for the evaluation of {adsorbent + adsorption process} systems are: purity, recovery, energy consumption and cost. In the case of CCS, a CO_2 purity of ≥ 95 $\%_{mol}$ is desired, and the highest recovery possible; 90 $\%_{mol}$ is generally taken. However, when comparing alternatives within a technology (*i.e.* various adsorbents) or between technologies (*i.e.* adsorption, absorption, membranes, distillation), the cost of undertaking the separation is the next key consideration. Process economics allows for trade-offs between capital and operating costs to be explicitly described. For instance, an adsorbent with poor working capacity may have higher capital costs attributed to adsorbent amount and adsorption vessels, however, it may show better performance at lower vacuum levels (higher absolute pressure), saving capital and operating costs for vacuum generation.

The evaluation of adsorbents accounting for these, and other, parameters is crucial, as it gives a more accurate representation of the attainable performance at scale. In the absence of experimental determination, these parameters can be accounted for by rigorous adsorption process simulation[20–29], or by reduced-order adsorption process models[30–34], as described in a number of CO_2 capture studies. Rigorous cyclic modelling can be arduous, especially regarding the cycle design and optimization. For what we aim to address here, *i.e.* swift adsorbent evaluation and screening, this approach is prohibitive owing to a typical paucity of available data. Reduced-order models are typically 0-D or

View Article Online
DOI: 10.1039/C9ME00102F

1-D equilibrium models which account for the aforementioned issues. These adsorption models are ideal for adsorbent screening as they are rapid and require minimum input data that can be easily obtained using common laboratory apparatus.

When applying these models, one should select the specific adsorption process, *i.e.* pressure swing adsorption (PSA), pressure vacuum swing adsorption (PVSA) temperature swing adsorption (TSA) or a combination of PSA and TSA (PTSA). All of these adsorption processes are cyclic, and in their simplest implementation, a mixture is passed through a packed bed of adsorbent where the more strongly adsorbed (heavy) component is removed, and the other (light) component passes through. Upon saturation of the adsorbent, the feed is diverted to another vessel and the saturated vessel is regenerated. In the case of PSA or PVSA this is by a reduction in pressure, and the more strongly adsorbed is collected as the other product. PSA or PVSA are commonly proposed as they have shorter cycle times than TSA processes, due to the lengthy cool down times of TSA beds. Given the vast volume of flue gases that are associated with large-scale post-combustion capture, short cycle times are key in reducing the amount of CO_2 that must be captured/stored per cycle – as there are the associated adsorbent requirements. PVSA – the approach selected for this work – also has the potential for much lower regeneration energy requirements than amine-based absorption processes[35]. This is due to the absence of both chemical reactions to be reversed, and the sensible heating requirements of the amine solution. A possible area of concern regarding packed-bed processes are the pressure drop limitations. Given the high volumetric flow rates, management of the pressure drop to avoid issues such as gas channelling and adsorbent crushing may result in a large number of vessels, as will be investigated in this work. An important aspect to consider when analysing a PSA/PVSA process is the variation of the adsorbent bed temperature. As adsorption is an exothermic phenomenon, the bed experiences a temperature increase during the adsorption step and a corresponding decrease during the desorption step. These temperature changes hamper the working capacity that the adsorbent has. Upon adsorption, the amount *adsorbed* is less than the isothermal (or feed temperature) amount. During desorption, the gas *recovered* is less than the isothermal amount.

View Article Online
DOI: 10.1039/C9ME00102F

This can result in a situation where the non-isothermal working capacity is significantly lower than that under isothermal conditions (or read off a single isotherm). While the desorption step is taking place, the composition of the gas and adsorbed phase also changes. As gas is removed from the adsorbent, this mixes with the existing gas in the bed, causing the composition to change. This means that the concentration of CO_2 at any point of desorption process is not the same as the feed concentration; thus, simple isotherm evaluation cannot give a reliable estimate. This is further complicated by the fact that the 'end composition' is not known *a priori*. The CO_2 concentration in the bed at the end of the desorption step is higher than the feed, thus the partial pressure is higher than imagined, also reducing the amount that can be removed from the adsorbent.

In our study, we have applied a PVSA model to screen 22 MOFs for CO_2/N_2 separation from post-combustion flue-gas sources from natural gas combustion, coal combustion, cement production, and steel production. We have screened MOFs using data reported in the literature and compared their performance and cost to that of commercial zeolites and activated carbon. Following this approach, we have determined links between adsorbent properties that influence aspects of the separation process (*i.e.* purity, recovery, and capture cost). We have also conducted a parametric evaluation of adsorbent properties to identify optimum adsorbent characteristics, and to generate a dataset that can be used by others to simply evaluate the performance of their adsorbents.

Our work evaluates adsorbents at scale without the necessity of intermediate scale-up steps. Those that are promising could be candidates for larger scale investigation, and rigorous adsorption modelling. This is accomplished while accounting for a range of industrially relevant factors, including separation performance, process equipment requirements, and cost. The association of adsorbent properties with these factors forms a link between materials science and industry; a pertinent requirement to accelerate the implementation of adsorption-based carbon capture technologies.

View Article Online
DOI: 10.1039/C9ME00102F

METHODS

Materials selection and cyclic adsorption model

We provide here a general overview of the model and describe the details in the Supplementary Information. The model includes three main sections, the PVSA model, equipment enumeration and sizing, and process economics.

The PVSA model determines the adsorbent performance under cyclic and adiabatic conditions. For this, we employ the 0-D equilibrium model developed by Maring and Webley[30], albeit with 500 steps used in the solution of the equations, rather than 100. This helps improve the accuracy of the result for materials with steep isotherms. The validation of the adsorption model was conducted in the original work, which found an acceptable match between experimental data and rigorous simulation results.

The model is equilibrium-based and its benefits over a kinetic-based model include: minimal input data, rapid solutions, and improved accuracy over simple metrics. Yet, opting for an equilibrium-based adsorption model has associated compromises. A kinetic model allows for bed profiles (*i.e.* temperature, pressure, composition) to be obtained, which leads to a more accurate simulation, and flexibility around the cycle operation – not possible with an equilibrium model. The timing of cycle steps can be optimised to maximise process performance. Another advantage of kinetic models is that all adsorbents can be modelled, however, experimentally determined mass transfer coefficients are required and these are generally obtained from breakthrough measurements. Breakthrough apparatus are fairly uncommon, and analysis of the data must be conducted carefully. In the absence of reliable adsorption kinetics data, efforts in cycle optimisation may be futile. Equilibrium models are valid only for adsorbents with sufficiently fast kinetics. It is therefore inappropriate to apply the model for adsorbents, which are known to have slow adsorption kinetics, such as K-A, K- or Cs-CHA, CMS, and supported amines at ambient temperatures. In summary, an equilibrium-based model allows a

View Article Online
DOI: 10.1039/C9ME00102F

first assessment of {adsorbent + process} systems, while a kinetic-based model enables a refined evaluation and a possible optimization of the process.

Adsorbents features and inputs – The PVSA model requires isotherms as a function of temperature and pressure for CO_2 and N_2, the density and void fraction of the bed, and the adsorbent heat capacity as inputs. One must have experimentally measured isotherm data while the other inputs can be approximated by various means, as detailed below. The availability of isotherm data in the literature at three temperatures for both CO_2 and N_2 represent the limiting factor in this work. In total, we investigated 22 MOFs along with an activated carbon, zeolite 13X and zeolite 5A. The 22 MOFs are in contrast to the approximately 86 that any gas adsorption data for CO_2 and N_2 were found in the literature, and to the many hundreds of reported MOFs without any reported gas adsorption data. The isotherm data, sources, and corresponding dual-site Langmuir isotherm fits are provided in the Supplementary Information. As a result of the limited information available, some of the adsorbents evaluated have stability issues in the presence of moisture, and other acid gas components in the flue gases. Yet, as will be explained in the cost analysis section, the annualised capture costs are substantial regardless of the MOFs, therefore, the inclusion of flue gas pre-treatment such as dehydration and desulphurisation will not alter the final conclusions.

The physical properties data for the adsorbents – *i.e.* density, bed void fraction, and heat capacity – are often unavailable and must be estimated. We used the desolvated crystallographic information files of the MOFs to derive some parameters. We determined the porosity of the adsorbent (ε_{ads}) using the solvent accessible pore volume; a probe with Connolly radius of 1.3 Å (helium) was used to obtain the occupied and free volume with the porosity obtained by applying Eq 4. From this, we calculated the total void space of the packed bed (ε_{bed}) by applying Eq 5, taking 0.37 (randomly packed spheres) as the packing void fraction (ε_{pack}). We estimated the pelletised adsorbent density (ρ_{pellet}) by applying a scaling factor of 80% to the crystallographic density; this relationship was established by Wu *et al.*[36]. We then quantified the density of the packed bed (ρ_{bed}) using Eq 6.

View Article Online
DOI: 10.1039/C9ME00102F

$$\varepsilon_{ads} = \frac{V_{free}}{V_{free} + V_{occupied}} \quad (4)$$

$$\varepsilon_{bed} = \varepsilon_{pack} + \left(1 - \varepsilon_{pack}\right) \cdot \varepsilon_{ads} \quad (5)$$

$$\rho_{bed} = \left(1 - \varepsilon_{pack}\right) \cdot \rho_{pellet} \quad (6)$$

The estimation of the heat capacity does not have an established method. We calculated the heat capacity of the MOFs by summing the molar fraction contributions of the metal atoms and the organic ligands. We used the molar heat capacity of the metal atoms from Rumble[37], and approximated the molar heat capacity of the organic ligands at 313.15 K following the method described by Goodman *et al.*[38]. A sample calculation is provided in the Supplementary Information. For the three reference materials, *i.e.* zeolite 13X, 5A, and activated carbon, the sources for their physical property data are provided in the Supplementary Information.

The reliance on reported isotherms as well estimated physical properties gives rise to uncertainties. Of the physical properties required in this work, the approach used for the MOF heat capacity has the most uncertainty. Using a molar fraction contribution of the metal atoms and ligands ignores the contribution of the lattice/crystal vibrational modes, thus underestimating the heat capacity. Conversely, the loss of some degrees of freedom of the ligand upon coordination is also not reflected, overestimating the heat capacity. The relative contributions of these factors are not known and will likely vary on a case-by-case basis. We therefore carried out a sensitivity analysis on the adsorbent physical properties and their influence on performance metrics (*i.e.* purity, recovery, and cost) and we discuss the findings in the results and discussion section. Uncertainty also exists in isotherm measurements[39–43], the root causes of this are multifaceted encompassing material synthesis, apparatus, and method. The utility of a sensitivity analysis on this is contentious, as isotherms repeated on the same sample on the same apparatus typically show little variation.

View Article Online
DOI: 10.1039/C9ME00102F

As our model relies on reported experimental isotherms, this approach takes advantage of the existing literature and accounts for 'real' structures rather than model ones. Yet, the requirement of having CO_2 and N_2 isotherms at 3 temperatures means that only a few materials can be investigated here.

Adsorption process features, inputs and outputs – We covered a wide range of CO_2 capture scenarios: a natural gas combined cycle flue gas (NGCC) a high rank pulverised coal ultra-supercritical flue gas (PC), a cement plant (cement), and an integrated steel mill (steel). The details of each scenario are provided in Table 1, with the sizes of each being typical scales of those plants. We determined the power plant flue gas flow rates and compositions using a procedure outlined in the Supplementary Information. The composition and flow rate data regarding the industrial capture applications are 'end-of-pipe' capture options proposed by the IEAGHG[44,45], where all flue gases are consolidated in to one stream.

Table 1 – Summary of post-combustion capture scenarios investigated in this work.

Scenario	Size	CO_2 concentration [mol·mol^{-1}]	Flow rate [kg·s^{-1}]	CO_2 emissions [MM t_{CO2}·yr^{-1}]
Natural gas	400 MW_e	4.38	607	1.28
Coal	500 MW_e	12.5	377	2.18
Cement	1 MM tpa	21.0	152	1.41
Steel	4 MM tpa	25.5	621	6.86

We considered an inlet gas pressure of 1.05 bar_a at a temperature of 313.15 K. The gas is then compressed to 1.50 bar_a and cooled to 313.15 K for adsorption. We investigated the influence of desorption pressure on adsorbent performance at five levels: 0.15 bar_a, 0.10 bar_a, 0.05 bar_a, 0.03 bar_a and 0.01 bar_a. These low vacuum levels are not necessarily industrially viable. We chose these levels in order to obtain the best possible performance (purity and recovery) from the adsorbents. If even at these vacuum levels, the performance is not reaching the desirable level, a change in the process is required.

View Article Online
DOI: 10.1039/C9ME00102F

We used the output from the PVSA model to size and enumerate the required process equipment. The PVSA model returns values on the basis of 1 kg of adsorbent and the process is scaled to the feed flow rate of each scenario, based on the total feed required to complete one adsorption cycle for 1 kg. As the PVSA model implemented here is an equilibrium model, cycle times are imposed *ex post facto*. We specified a 1-hour total cycle consisting of 45 minutes adsorption/feed time, and 15 minutes desorption time. This is compared to ≤ 15 minutes for PSA systems used for H_2 production or air separation. The cycle time is the main contributor to process intensification: fewer adsorbent vessels are required if the cycle time is reduced. This is due to the requirement to accommodate the adsorbing species in the feed for the duration of the adsorption time. The volumetric flow rate of the feed gas dictates the line and valve sizes, which for large-scale post-combustion capture, is inherently high. This necessitates large pipe diameters and valves, generally motor actuated, with slow actuation times (5 – 10 minutes). Thus, switching flow paths between cycle steps is time consuming. In the instance where one bed is being switched from adsorption to regeneration, the feed must be diverted to the regenerated column prior to shutting off the saturated one. These factors culminate in a situation where cycle times < 30 minutes for these situations are highly unlikely. As detailed design data is unknown, we have assumed a cycle time of 1 hour to account for these factors while also allowing for some margin in the operation.

Process economics

The primary equipment items included in the capital cost calculations are the feed gas compressor, feed cooling exchangers, adsorbent vessels, adsorbent, and vacuum pumps. The minor equipment items included are the cooling water pumps, vacuum pump motors, and control valves directly associated with the adsorbent vessels. The operating costs cover the electrical requirements for the rotating machinery, cooling water requirements, and adsorbent replacement costs.

For the purposes of comparison, we assigned all adsorbents a cost of 1.5 £·kg^{-1} and a lifetime of 5 years. Some MOFs have chemical and thermal stability issues and/or are costly to synthesise due to

View Article Online
DOI: 10.1039/C9ME00102F

the requirement for exotic organic ligands, rare metals, and solvent use. Therefore, it may be naive to assume that all MOFs have the same lifetime of 5 years. Adsorbents currently applied industrially such as zeolites, activated carbons, and silicas and aluminas, display lifetimes of 7 – 10 years if the process is operated sensibly. As there are no long-term studies of MOFs being applied at the pilot scale for adsorption-based processes, we have opted for a conservative estimate based on existing knowledge, while also giving the MOF materials the best chance. The cost of 1.5 £·kg^{-1} is in-line with industrial purchase costs for zeolite 13X from generic manufacturers, with costs being up to 3.5 – 5 £·kg^{-1} for the state-of-the-art materials from the eminent manufacturers. If a MOF is deemed suitable for carbon capture applications and is commercialised, raw material production can be scaled to the requisite level with existing technologies. An assigned value of 1.5 £·kg^{-1} assumes that MOF production could be scaled efficiently and is the best-case scenario cost for a synthetic adsorbent. As per the physical properties, the influence of adsorbent cost on capture cost was investigated in our sensitivity analysis (See Results and Discussion).

We converted the electrical requirements to an equivalent cost of natural gas that would need to be combusted in an on-site boiler to produce that electrical power. We did not include these outside battery limits (OBL) costs in the separation plant capital costs.

We determined the installed costs using the IChemE/factorial cost estimation method[46,47] with equipment purchase costs taken from a range of sources detailed in the Supplementary Information. We adjusted the costs for economic factors using the Chemical Engineering Plant Cost Index (CEPCI). Values reported in this work are based on the October 2018 value of 616.3, and a USD to GBP exchange rate of 0.76 £·$^{-1}$. There are limitations in the costing approach proposed here (accuracy is ±30 %). Yet, such approach allows us to make a more informed conclusions with the data that is currently available.

To determine the cost per tonne of CO_2 captured, we used the total annualised cost (TAC), Eq 7, where CRF is the capital recovery factor and C_{Cap} and C_{Op} are the total capital costs and annual operating costs, respectively.

$$TAC = CRF \cdot C_{Cap} + C_{Op} \quad (7)$$

View Article Online
DOI: 10.1039/C9ME00102F

For the capital recovery factor (Eq 8), we assumed a cost of capital (i) of 10 %, and a repayment period (n) of 25 years.

$$CRF = \frac{i \cdot (1+i)^n}{(1+i)^n - 1} \quad (8)$$

The costs of capture for each scenario using amine absorption to achieve 90 % CO_2 capture were also determined as a point of comparison. Costs for 30 $\%_{wt}$ monoethanolamine (MEA) and a 'new generation' ('NG') absorbent with lower regeneration energy requirements such as Cansolv[48]. A cost of 1100 US$\cdot t^{-1}$ was used for both amine absorbents. The details of the model are provided in the Supplementary Information. A conventional process topology is used with multiple unit operations were required due to equipment size limitations (heat exchanger areas and column fabrication limitations).

The flue-gases are assumed to be provided dry and without contaminants, with the drawback that pre-treatment equipment and costs are not accounted for in this work. The implications of this are not significant in this case as explained in the results and discussion section.

The majority of the work on post-combustion capture *via* adsorption has been focused on coal-fired sources, likely due to their more manageable CO_2 content. Indeed, the higher CO_2 content in coal-fired flue gases means that the separation is easier to achieve. These reported economic assessments[49,50] provide comparison points for our work. We have observed significant variation between these reported estimates and our work (3 to 10 times). The cost differences between our work and that of Susarla *et al.*[50] likely arose from the differences in the cost of vessels and vacuum pumps. In our case, we calculated the cost of adsorbent vessels based on mass of steel required, which is determined using the relevant pressure vessel standards. The vessels must withstand vacuum, which results in high vessel thicknesses and a correspondingly high mass. For vacuum pumps, we opted for an equipment cost correlation from Garrett[51]. Susarla *et al.* used cost correlations for the vessels based

View Article Online
DOI: 10.1039/C9ME00102F

on volume, which ordinarily do not account for the pressure vessel requirements, and they obtained costs for vacuum pumps from vendors. Considering vessels and vacuum pumps comprise the greatest proportion of capital costs, differences in the determination of these could result in significant variation. Indexing of costs to current day values was also not mentioned in either case.

RESULTS AND DISCUSSION

Adsorbent evaluation and screening

Applying the model described above, we have screened 22 MOFs, 2 zeolites and an activated carbon for the CO_2 capture scenarios mentioned earlier (Table 1). We show the outcomes for all scenarios in Figure 1. We describe in detail the NGCC case first and then provide a broader overview on the other scenarios. In Figure 1, we have grouped the adsorbents in the following way, Mg-MOF-74 through UTSA-16 are MOFs with open metal sites, MOF-177 through Zn(BPDC)(BPP) are those with fully saturated coordination sites, ZIF-8 through ZIF-82 are the sub-classification of MOFs known as zeolitic imidazolate frameworks, and activated carbon through zeolite 13X are commercial adsorbents for reference.

NGCC case – Zeolite 13X and UTSA-16 display the best results in terms of purity and recovery (69 $\%_{mol}$ and 81 $\%_{mol}$ respectively at 0.01 bar_a). Mg-MOF-74, one of the most often cited MOFs for CO_2 capture[17], appears as a very poor adsorbent for this process (24 $\%_{mol}$ and 37 $\%_{mol}$ respectively at 0.01 bar_a). These results highlight particularly well the limitations of simply considering CO_2 uptake as a relevant metric; this aspect is discussed further below. For all adsorbents, deep vacuum is required to obtain any noticeable improvements in CO_2 recovery, and purities are generally low.

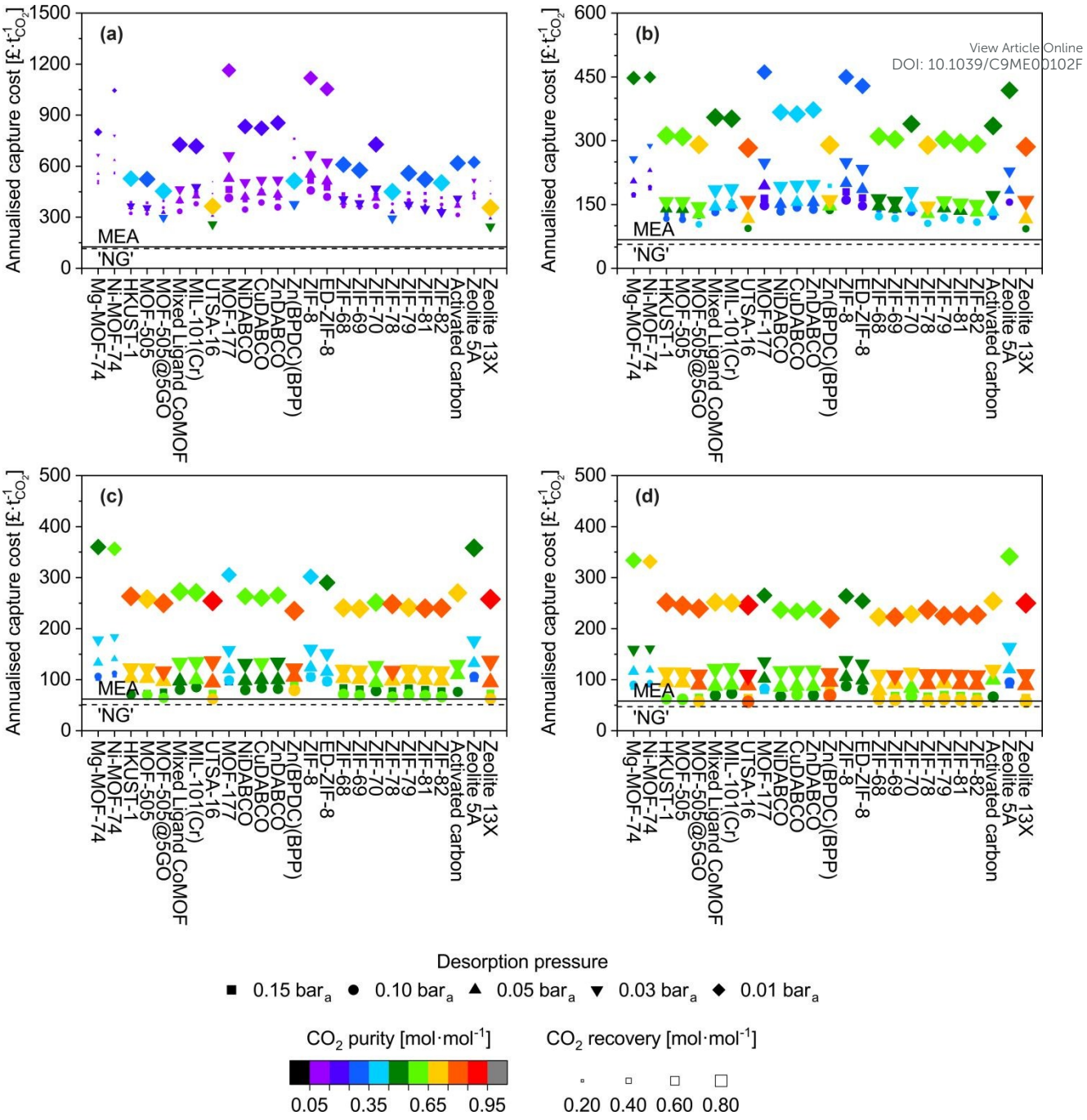

Figure 1. Separation performance and cost evaluation of 25 adsorbents for CO_2/N_2 separation for the four scenarios investigated as a function of desorption pressure: **(a)** NGCC, **(b)** coal-fired, **(c)** cement, **(d)** steel. In all cases, the cost of the MOFs is taken as £1.5 kg^{-1}.

The most striking output is the capture cost, with most data points > 300 £·t^{-1}, while amine absorption is below 150 £·t^{-1}. These costs may seem initially higher in comparison to other reports[52–57]. In all those cases, single equipment items are used and sized without limitations. In our work,

View Article Online
DOI: 10.1039/C9ME00102F

limits are imposed on maximum column diameter, heat exchanger area, feed blower flow rate *etc.* resulting in multiple unit operations. The full details of this are provided in the model description in the Supplementary Information, however, the result of this is that capital costs using our approach are high.

The adsorption high costs are capital driven, and a breakdown of the costs are presented in the Supplementary Information (Figure S1 to S4). One reason for this is the feed gas is low density and correspondingly the volumetric flow rate is significantly high. Accommodating the recommended gas velocities and pressure drops in the adsorption columns necessitates several columns in parallel to distribute the feed. Low velocities (*i.e.* pressure drop per unit length) will result in gas channelling and poor distribution of gas through the bed. Conversely, high overall pressure drops (*i.e.* total pressure drop of the packed bed) can crush the adsorbent pellets. Vacuum pumps also contribute significantly to the capital costs. Normally, large-scale vacuum generation is achieved using steam ejectors, however, the product becomes mixed with steam. The limitation of mechanical vacuum pumps is the maximum achievable flow rate. The variant opted for here has a maximum flow rate of ≈15,000 act.$m^3 \cdot hr^{-1}$. However, given that the desorption step is a fraction of an hour (in this case 15 minutes), multiple parallel pumps are required to achieve the nameplate flow rate. Furthermore, at 0.01 bar_a, a given number of moles of gas occupies ≈100 times more volume than at standard conditions.

The adsorbent working capacity also contributes to the number of columns. Adsorbents such as MOF-177 and ZIF-8 have low capacities and linear isotherms in the pressure range of interest[58,59]. This results in a low working capacity which necessitates a considerable adsorbent mass, and corresponding vessel volume to adsorb the captured CO_2.

Other cases – We now turn our attention to the other scenarios. We provide a more brief analysis for those since the same theories as the NGCC case apply (Figure 1). All cases exhibit better purities, recoveries and costs compared to NGCC. This observation is globally attributed to the higher CO_2

View Article Online
DOI: 10.1039/C9ME00102F

concentration in the flue gas, resulting in an easier separation. This aspect is also reflected in the working selectivities with many more adsorbents displaying values above unity (Figure S9 to S12). The increased feed concentration from approximately 4 $\%_{mol}$ CO_2 not only increases the CO_2 working capacity for adsorbents with more linear isotherms, the associated decrease in N_2 concentration means N_2 adsorption is also reduced. The relationship to capture cost is not as straightforward since the flow rates between each case are not consistent, and neither are the obtained purity and recovery values. In general, the increased CO_2 recovery for most adsorbents is a major contributor to the reductions in cost, and further capital cost reductions are seen due to the lower gas flow rate. Yet, the cement and steel scenarios display similar cost despite significantly different flow rates. Increasing CO_2 concentration has limited benefit on M-MOF-74 adsorbents (*i.e.* steep isotherms) as they transition into the saturated area of the isotherm. The initial improvement in performance – from the NGCC to the coal scenario – stems from the transition from the saturated region of the isotherm to the steeper region during desorption, thereby increasing the working capacity. Most of the other MOFs display gradual isotherms and these higher partial pressures result in improved working capacities. For the cement and steel scenarios, the 0.01 bar_a desorption points are grouped fairly well together. This is mostly coincidental as there is no trend in the numerical data that suggests it is due to a given factor. The specific combination of CO_2 working capacity, CO_2 recovery, and vacuum flow rate required for each adsorbent has resulted in this grouping with improvements in one value being offset by another.

In addition to purity and recovery, another commonly used performance indicator is the energy penalty, or parasitic energy of the plant. We have included plots of energy penalty for all scenarios in the Supplementary Information (Figure S5 to S8). For UTSA-16, the total power and specific energy range from 83 MW and 1.96 $GJ_e \cdot t_{CO2}^{-1}$ in the cement scenario to 377 MW and 1.82 $GJ_e \cdot t_{CO2}^{-1}$ for the steel scenario at 0.01 bar_a desorption pressure. The power requirements are affected by the feed flow rate differences, and the specific energy requirements may be a better comparison between separations. For the natural gas and coal scenarios, specific energies of 4.1 and 2.4 $GJ_e \cdot t_{CO2}^{-1}$, respectively, are required.

View Article Online
DOI: 10.1039/C9ME00102F

The scenarios investigated here do not highlight any grouping within the MOF families. This suggests that there is not a singular adsorbent factor or characteristic that defines the suitability of an adsorbent for a given application. This is not necessarily surprising as working capacity, recovery, and working selectivity are the parameters that define process performance and cost. It is not unforeseeable that a multitude of isotherms could yield the same results. For instance as previously mentioned, UTSA-16 and zeolite 13X display very similar performance, however, they are very different in nature. This hypothesis is tested later in this study.

Comparison of performance and cost with respect to targets – Of the 22 MOFs investigated, none under any of the conditions investigated here display CO_2 purities ≥ 95 $\%_{mol}$, which is the level generally considered acceptable for CCS. UTSA-16 displays similar performance to 13X in this work, and 13X has been shown to achieve purities ≥ 95 $\%_{mol}$ and recoveries ≥ 90 $\%_{mol}$[60,61] for coal-fired post-combustion capture. This comparison highlights the possible improvement brought by cycle optimization, an aspect we discuss in a latter section. The choice, and more importantly, the optimization of the adsorption cycle used significantly impact the attainable results[62]. The same cycle (*i.e.* sequence of steps) that is operated or designed (*i.e.* flow direction, step times, intermediate pressures, *etc.*) by different people will yield different results. A complex cycle poorly optimised may yield worse results than a finely tuned simpler cycle. Complex cycles add significant capital cost due to the multiplicity of columns required. If the ratio between total feed time and desorption time are equal, *i.e.* 75 % of total cycle time is adsorption time, a 6-bed cycle would require six times the number of beds of the cycle used here. Considering UTSA-16 for the coal case requires 47 beds at best, although it may be technically feasible, it will not be economically or spatially feasible for these high flow rate applications.

We now provide a perspective on costs with comparison to the costs of amine absorption. All scenarios here cost more than amine adsorption, though we find exceptions for cement and steel at 'high' desorption pressure (0.10-0.15 bar_a). For the lowest desorption pressure (0.01 bar_a) for which

View Article Online
DOI: 10.1039/C9ME00102F

the best performance in terms of purity and recovery are seen, the costs remain significantly higher than the benchmark. There are two main contributions to this. The first is the superior gas handling capability of absorption columns relative to packed columns. A given diameter can accommodate a higher flow rate with lower pressure loss. For the 0.01 bar_a case, the vast majority of the costs are vacuum equipment capital costs, which are unavoidable in a PVSA system. Finally, the amine absorption process achieves a recovery of 90 $\%_{mol}$ and purities $\geq$ 95 $\%_{mol}$ CO_2, it is therefore an unfair comparison to a certain extent but further demonstrates that for these large-scale applications, PVSA may not be the optimal choice. The use of MEA based absorbents as a benchmark is also somewhat outdated as there are new systems based on mixtures of methyl diethanolamine (MDEA) and piperazine (PZ), and 2-amino-2-methyl-1-propanol (AMP) and piperazine, which display more desirable characteristics[63] and may have lowered capture costs even more. Given the costs presented thus far, pretreatment and product compression costs are not an immediate concern. However, examples of these costs can be found in a range of resources[64–66].

From an adsorbent perspective, of the MOFs evaluated, UTSA-16 does appear to perform the best for the post-combustion capture scenarios investigated using PVSA. Its performance is on par with zeolite 13X over all factors considered here. Considering its water co-adsorption and regeneration characteristics are more desirable than zeolite 13X,[67–69] it may be a preferred candidate assuming that long-term cyclic stability can be verified. It is possible that the MOFs investigated here display better performance in a TSA process. However, conventional TSA processes have long cycle times due to the cooling of the vessel. This results in a greater number of columns to continuously accommodate the feed. Yet, this may be offset by the absence of vacuum costs. Whether suitable process intensification can be achieved will determine the feasibility of conventional TSA processes for large-scale applications. If recent developments in TSA technology such as Inventys' VeloxoTherm™ process[70] are successful, it may enable industrial scale application of TSA for post-combustion capture.

View Article Online
DOI: 10.1039/C9ME00102F

From the screening exercise above, we conclude that: (i) MOFs performed poorly relative to amine-based absorption for the selected CO_2 capture scenarios, though we observe improvements for more concentrated feeds and further improvements could be brought by process optimization; (ii) UTSA-16 performs the best out of all the MOFs screened while Mg-MOF-74 performs unsatisfactorily; (iii) the former observation highlights how the evaluation methods used in the existing literature are typically unfitting to claim a given MOF is suitable for CO_2 capture applications.

UTSA-16 *vs* Mg-MOF-74

We investigate here in more details the underlying reasons for the distinct performances of these two MOFs. This 'exercise' allows us to get a first grasp on the links between material properties and process performance. The isotherms of USTA-16 and Mg-MOF-74 are shown in Figure 2. Mg-MOF-74 exhibits steep isotherms and a high enthalpy of adsorption, leading to two compounding effects. The steep isotherms require very deep vacuum to desorb the adsorbed gas. Since the process is adiabatic, a high enthalpy of adsorption causes greater temperature increase in the bed upon adsorption, reducing the capacity, and the corresponding decrease upon desorption retains the adsorbed gas. The bed temperature swing, *i.e.* the difference between the highest and lowest temperature experienced, is 25 K for Mg-MOF-74, *vs* 5 K for UTSA-16 at 0.01 bar_a desorption. Comparing the isotherms in Figure 2, it also becomes apparent that ultimate CO_2 capacity is not necessarily significant. In fact, working capacity drives the low recoveries seen in many cases. Indeed, although Mg-MOF-74 has excellent CO_2 capacity, it does not perform well when regenerability is accounted for. Considering the cyclic nature of the adsorption process, regenerability/desorption has equal importance as adsorption.

The excellent CO_2 adsorption of Mg-MOF-74 is also accompanied by high N_2 adsorption. This is due to the large pore apertures and high surface areas, which result in the adsorbent being non-discriminatory. In such a case where there is ≈96 $\%_{mol}$ N_2 in the feed, N_2 adsorption becomes an area of concern. The adsorbed N_2 is collected with the CO_2 product, and as such, any N_2 adsorbed dilutes

View Article Online
DOI: 10.1039/C9ME00102F

the CO_2 product. This is further enhanced by the fact that N_2 is easier to desorb than CO_2, and in many cases the working capacity of N_2 can be greater than CO_2. The greater purity results displayed by UTSA-16 are not solely due to better CO_2 working capacity, but also due to excellent selectivity. For the purposes of comparison, a plot of the ratio between the CO_2 and N_2 working capacities, also known as the working selectivity, is included in the Supplementary Information (Figure S9 to S12) for all adsorbents. It shows that most of the MOFs are hampered by poor selectivity. This analysis highlights that one should look at enhancing CO_2/N_2 selectivity and decreasing the N_2 uptake rather than maximizing CO_2 uptake.

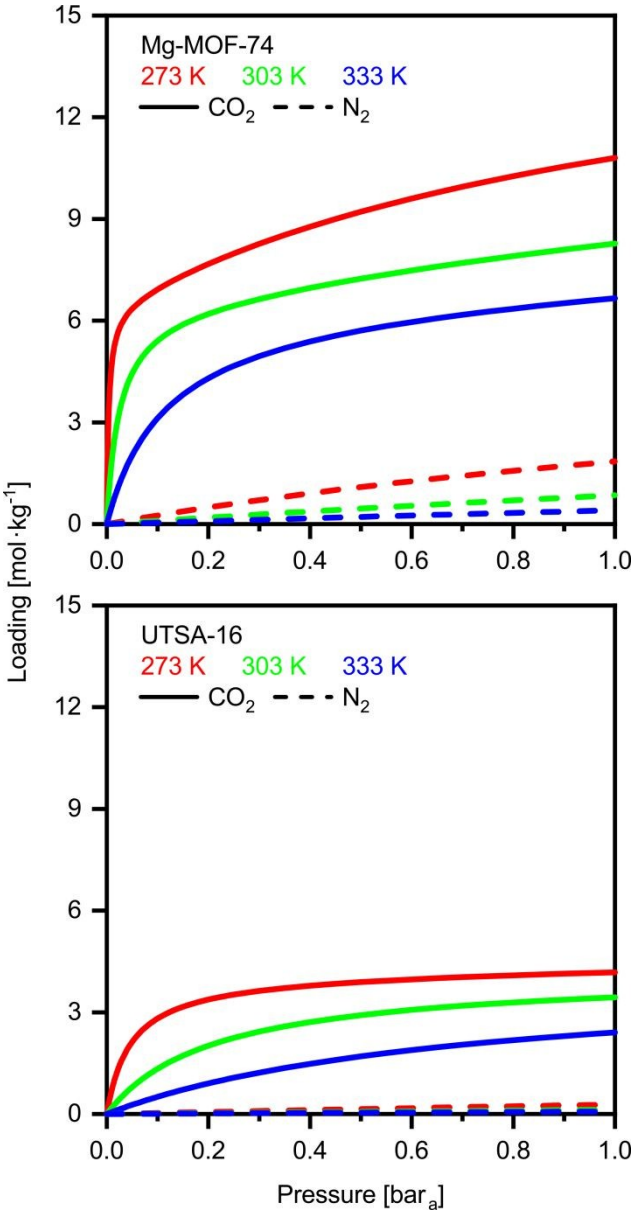

View Article Online
DOI: 10.1039/C9ME00102F

Figure 2. CO_2 (solid lines) and N_2 (dashed lines) adsorption isotherms of the two 'extreme' MOF adsorbents in terms of separation performance: Mg-MOF-74 (top, poorly performing MOF) and UTSA-16 (bottom, highly performing MOF) at 273 K (red), 303 K (green), and 333 K (blue).

Effects of process parameters

Taking Mg-MOF-74 and USTA-16 as examples, we then investigated the effect of process and adsorbent parameters on performance and capture cost, namely: adsorption temperature, desorption pressure, adsorbent cost and adsorbent density.

We first investigated the impact of adsorption temperature, *i.e.* the temperature the feed is adjusted to following compression, on the purity, recovery and cost. The results are presented in Figure 3a-c. Considering all three outputs, Mg-MOF-74's performance is optimum between 358 and 373 K. CO_2 purity increases with temperature up to 373 K due to two factors: higher temperature isotherms are less steep, which improves the working capacity, and the nitrogen loading is suppressed. Beyond 373 K, the CO_2 purity reduces due to the CO_2 working capacity decreasing at a rate faster than the reduction in void volume. The improvement in recovery with temperature is also due to the isotherms becoming less steep. The minimum capture cost is seen at ≈373 K, *i.e.* when the improved working capacity and recovery and the corresponding reduction in capital costs offset the increased operating costs to supply steam for feed heating. Beyond this point, the increased heat exchanger area and steam utility required to heat the feed are further disadvantaged by reductions in working capacity and recovery – resulting in a higher cost per tonne captured. The CO_2 emissions from the generation of the steam should also be kept in mind. The optimum temperature for UTSA-16 is seen at 313 K, *i.e.* the current operating temperature. Changes in temperature either side will reduce the CO_2 working capacity, resulting in poorer purity, recovery, and capture cost. For completeness, we present an extended temperature range in the Supplementary Information (Figure S16 to S20) for all adsorbents. Only results for purity and recovery are shown, as the requisite allowances to calculate the cost under cryogenic operation are not present in the model. In summary, tuning the adsorption temperature may

allow to reach higher performance levels, though in the present cases, the outputs remain below the targets.

View Article Online
DOI: 10.1039/C9ME00102F

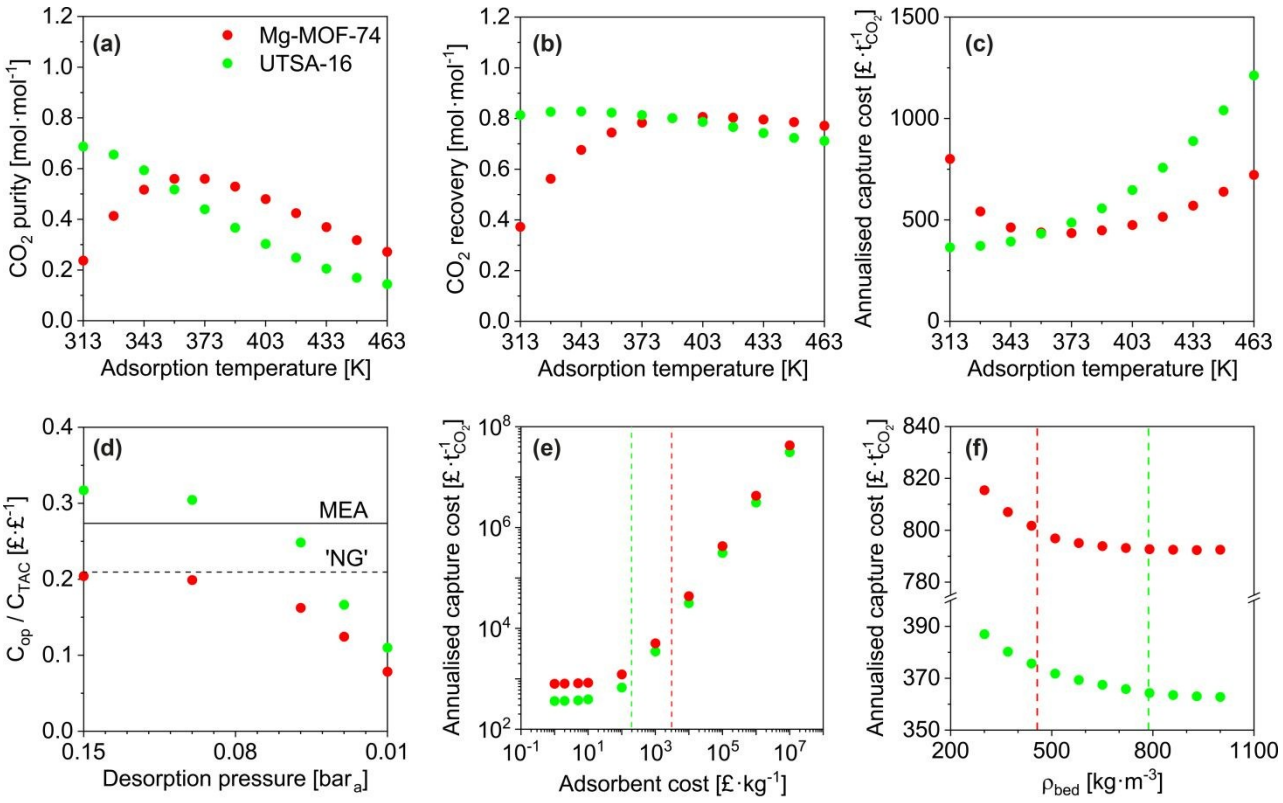

Figure 3. Evaluation of the effect of process parameters on separation performance and cost for Mg-MOF-74 (red) and UTSA-16 (green). Influence of adsorption temperature on: (a) CO_2 purity, (b) CO_2 recovery, and (c) capture cost. (d) Influence of desorption pressure on annual fraction of operating costs, where 'NG' represents Cansolv. (e) Influence of adsorbent cost on capture cost. (f) Influence of adsorbent density on capture cost. All for the NGCC scenario. All at 0.01 bar_a desorption pressure, except (d).

Figure 3d shows the fraction of operating costs over total annual costs as a function of desorption pressure. This fraction reduces with decreasing desorption pressure and is solely due to the increasing capital costs due to the vacuum requirements. A range of adsorbents, including Mg-MOF-74, displays a maxima, caused by vacuum pump capital costs. Higher desorption pressures reduce the suction flow

View Article Online
DOI: 10.1039/C9ME00102F

rate of the vacuum pump selected. Consequently, a greater number of pumps are needed to achieve the required flow rate. Data for the other adsorbents is included in Figure S21.

Figure 3e presents the influence of adsorbent cost. As other significant capital costs contribute to the process, the cost of the adsorbent does not become significant until 50 – 100 £·kg^{-1}. In systems where adsorption is currently applied, *e.g.* air separation and H_2 production, the capital costs are significantly lower, so the cost of the adsorbent can impact the separation cost. However, for post-combustion capture, the current MOF cost target value[71] of 10 US$·kg^{-1} does not have to be reached to minimise the separation cost. It should be noted that this cost was proposed by the US DOE for CH_4 storage in vehicles, however, it seems to have propagated through the community. We determined the cost of UTSA-16 (196 £·kg^{-1}, vertical line on the plot) and Mg-MOF-74 (3070 £·kg^{-1}) using prices for bulk chemical supply from common scientific suppliers and yields reported in the literature. We calculated the cost of zeolite 13X (66 £·kg^{-1}) following the same method. Using the latter cost as an indicator of economies of scale to the industrial 13X price of 1.5 £·kg^{-1}, this implies that UTSA-16 might be produced at a cost of 5 £·kg^{-1}. The largest limitation in the synthesis of UTSA-16 is the metal source, cobalt acetate, as all other raw materials are readily available at scale. It may therefore be worth investigating the possibility of isoreticular chemistry for UTSA-16, and whether a more accessible metal source such as Zn^{2+} or Fe^{2+} is possible while maintaining similar adsorption properties.

Quantitative results for the impact of adsorbent density on cost are shown in Figure 3f. As addressed during the sensitivity analysis, the cost increases as the adsorbent density decreases. The benefits of a dense adsorbent are seen for UTSA-16. For Mg-MOF-74, significant cost reductions are not necessarily attainable even if pelletisation were used to increase density. This is ultimately due to the poor CO_2 recovery of Mg-MOF-74. The recovery defines the total mass of CO_2 that is captured from the feed, and the working capacity defines the amount of adsorbent required to capture that amount of CO_2. Hence, the poor recovery implies a small mass of adsorbent. As the density increases, the vessel volume required to store that adsorbent reduces. A point is reached for Mg-MOF-74 such that

View Article Online
DOI: 10.1039/C9ME00102F

it is not possible to reduce the number or size of the vessels further while still meeting the velocity and pressure drop requirements.

Finally, we evaluated the impact of feed flow rate on the approximate site area required for the plant. We conducted this study in the context of the NGCC scenario and using USTA-16 properties. As seen in Figure 4, the 400 MWe case calls for an area of ≈18,000 m^2. This area only accounts for the number of adsorption columns and vacuum pumps required, while allowing a 0.5× spacing between the equipment items. Once all other equipment items such as compressors, heat exchangers, pumps, and OBL plant is included, the total area may be 1.5 – 2× this value. The default comparison to a range of stadia has also been included. Jest aside, reduction in the plant area is paramount in the successful implementation of adsorption for post-combustion capture. Efforts should be placed towards process intensification and improvements in mechanical vacuum generation technology.

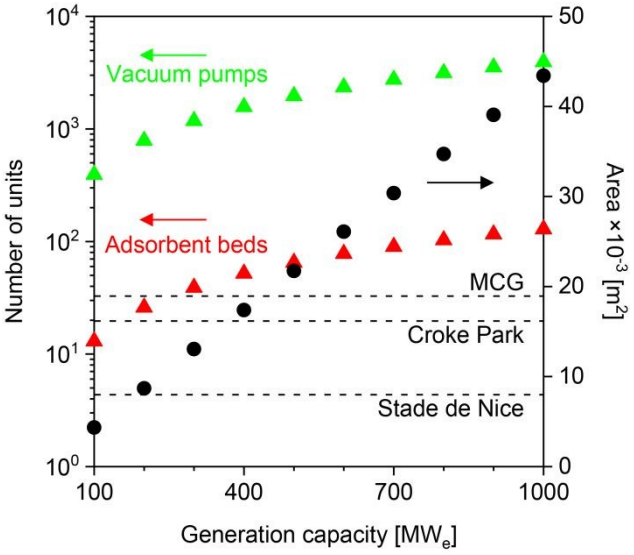

Figure 4. Area occupied by vacuum pumps and adsorption columns as a function of power generation capacity (flue gas flow rate) for the NGCC scenario, using UTSA-16 as the adsorbent.

Sensitivity analysis

As previously mentioned, there may be some uncertainty in the adsorbent physical properties as they are not experimentally measured or verified values but estimated ones. To investigate the

View Article Online
DOI: 10.1039/C9ME00102F

implications of inaccuracies in bed density, void fraction, and heat capacity, we carried out a sensitivity analysis over a ±30 % range for each property while keeping the others constant (Figure 5 and Figure S13 to S15). Due to the interrelated nature of adsorption processes, we investigated the effect of the three physical property inputs for both Mg-MOF-74 and UTSA-16 at two desorption pressures. Upon first observation, variations in adsorbent density and void fraction do not have significant influence on any of the three performance metrics, while heat capacity does to some extent.

We now examine these observations in greater detail. The density and void fraction both contribute to the total amount of void space present in the bed for a given mass of adsorbent. The void space impacts the dilution of the desorbed product gas (CO_2) by the feed gas occupying the void space. Therefore, in general, a larger void volume results in poorer product purity. This is seen for all scenarios presented below, a reduction in void fraction improves CO_2 purity, and *vice versa*. An increase in density also improves CO_2 purity. The largest impacts are observed at the lower desorption pressure. Although a lower desorption pressure recovers more CO_2 from the adsorbent positively contributing to purity, the lower pressures also recover more of the approximately 96 % N_2 present in the void space.

Unlike density and void space, variations in the heat capacity significantly affect the performance of Mg-MOF-74 at 0.01 bar_a. The effect is not as severe at higher desorption pressures, nor is it significant for UTSA-16. To explain this observation, we compare the adsorbents and operating conditions. The first contribution is due to the difference in enthalpy of adsorption between the two adsorbents. Mg-MOF-74 has an enthalpy of adsorption at zero loading for CO_2 of at least 47 $kJ \cdot mol^{-1}$ [17,72], whereas UTSA-16 is ≈32-35 $kJ \cdot mol^{-1}$ [73]. If the actual heat capacity is lower than the estimated value (negative x-values), the bed experiences a larger temperature swing for a given energy input/output. As these swings are already large for Mg-MOF-74, a further increase has even worse implications on the CO_2 purity and recovery, reducing the working capacity even further. The reverse applies for the improvements in purity and recovery seen in the right direction of the axis, a higher adsorbent heat capacity limits the temperature swing. The contribution of desorption pressure to this

View Article Online
DOI: 10.1039/C9ME00102F

observation is related to the working capacity/amount desorbed. At higher desorption pressures, fewer moles of gas desorb, thus requiring smaller thermal energy input from the surroundings to do so; therefore, variations in heat capacity are less significant. As the amount desorbed is not a linear function of pressure (logarithmic isotherm shape), the influence of heat capacity does not have a linear relationship with desorption pressure.

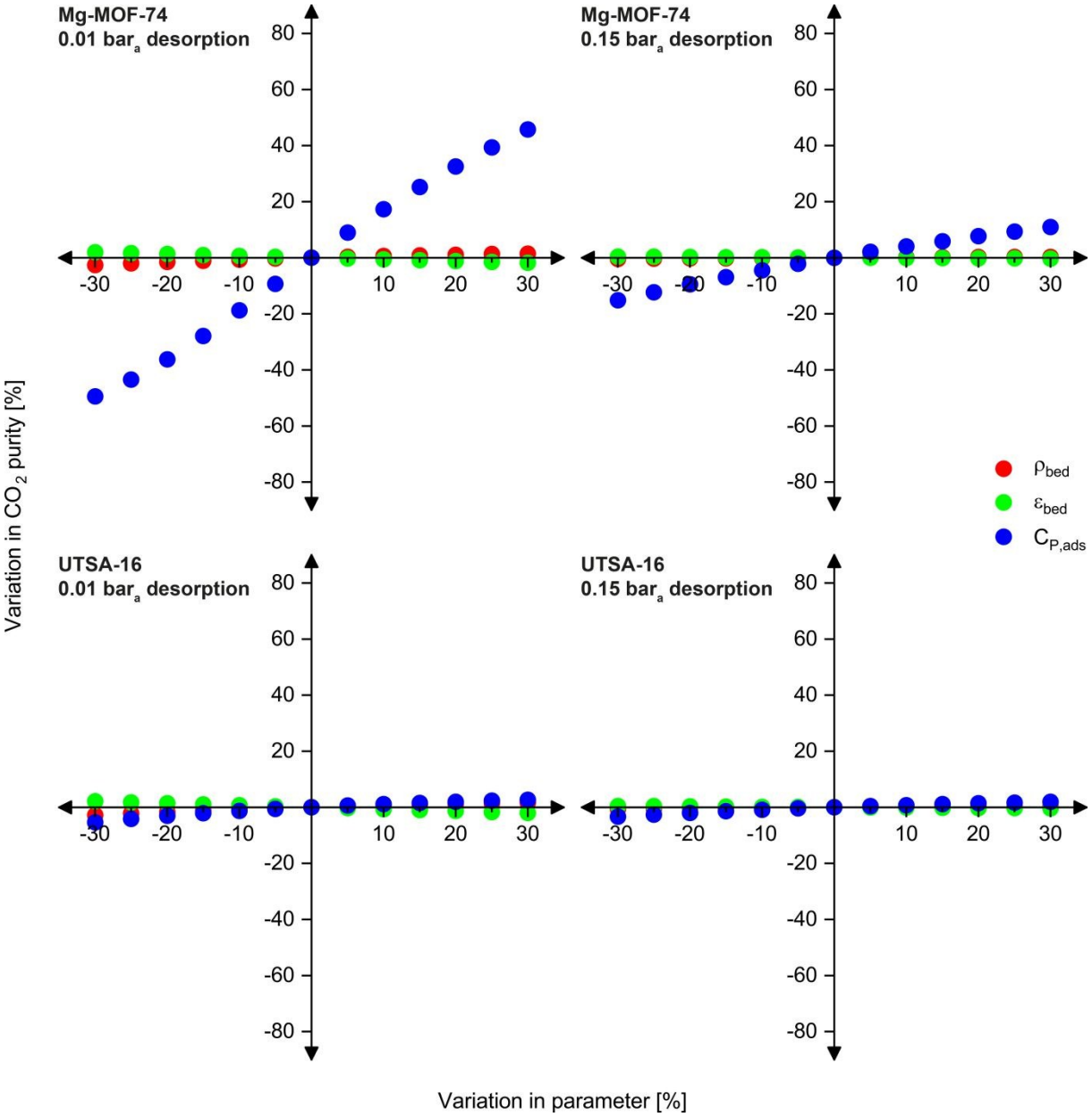

Figure 5. Sensitivity analysis of adsorbent physical properties (density, void fraction, and heat capacity) on CO_2 purity for Mg-MOF-74 (top) and UTSA-16 (bottom) at 0.01 bar_a desorption (left) and 0.15 bar_a desorption (right).

View Article Online
DOI: 10.1039/C9ME00102F

In some cases, these effects combine in a beneficial (and convoluted manner), such as the CO_2 recovery for UTSA-16 at 0.15 bar_a (Figure S14). The feed required to complete one cycle decreases due to the lower heat capacity of the adsorbent resulting in a greater temperature swing of the bed. However, a natural feedback loop exists where desorption becomes more difficult as it proceeds, due to the concurrent reduction in temperature. As desorption is taking place at a higher pressure, the working capacity of CO_2 is not significantly reduced as a balance is met between higher temperature change from reduced heat capacity, and lower temperature change due to higher desorption pressure. As CO_2 recovery is defined as the ratio of CO_2 product to total CO_2 feed, this culminates in higher CO_2 recovery. This is not observed for all adsorbents and is normally caused by the combination of heat of adsorption, and the relative amounts of gas removed from the void space and from the adsorbent. This is seen in the effect of void fraction on CO_2 recovery for UTSA-16 at 0.15 bar_a desorption. A lower void fraction results in lower CO_2 recovery, which suggests that a reasonable portion of the 'working capacity' is coming from the feed CO_2 occupying the void space, rather than what is collected from the adsorbent.

Considering now capture cost, lower densities increase costs due to: (i) the larger size of the vessels needed to accommodate the mass of adsorbent, and (ii) the greater amount of vacuum capacity required. In general, a lower void fraction reduces capital costs since the adsorbent occupies a greater portion of the adsorption vessel volume and requires reduced vacuum capacity. The UTSA-16 result for 0.15 bar_a desorption represents an exception. Due to the aforementioned reduction in recovery, a greater mass of adsorbent is required to capture the given feed flow rate, resulting in higher capital costs for vessels and adsorbent.

Overall, variations in the adsorbent density and void fraction do not influence significantly the performance and costs of the capture process. Heat capacity, on the other hand, may have an impact for adsorbents with high enthalpies of adsorption, such as Mg-MOF-74. We note that these implications remain relative. For instance, although an improvement of ≈46 % can be seen in the CO_2

View Article Online
DOI: 10.1039/C9ME00102F

purity at 0.01 bar_a if the heat capacity were underestimated by 30 %, the ultimate outcome of this is that the CO_2 purity increases from 23.7 $\%_{mol}$ to 34.5 $\%_{mol}$, which remains low.

Optimising adsorbent properties

Having developed a reasonable understanding of the process and the factors which influence process performance, we will now direct our attention to the adsorbents themselves. Our goal here is to identify and quantify the adsorbents characteristics needed to push the performance and capture cost towards the targets. This theoretical exercise, conducted on Mg-MOF-74 and USTA-16, will provide directions to chemists and materials scientists in the design and synthesis of highly performing adsorbents. This has been attempted by others to a certain extent[30,49,74,75], where hypothetical adsorbents (or isotherms) are proposed to optimise separation performance. Aside from the impact on process economics, which the majority do not address, we propose some synthesis routes by which the optimum properties could be obtained. We note that limiting the analysis to the extreme cases of Mg-MOF-74 and USTA-16 will not necessarily exclude any of the MOFs from the original list. Indeed, Mg-MOF-74 has large surface area and porosity and strong open metal centres, whereas UTSA-16 is a small pore adsorbent with low(er) porosity and more moderate enthalpy of adsorption. Thus, the majority of the other adsorbents should be incorporated in that range.

Adsorption isotherms provide a reflection of an adsorbent's physical and chemical properties. Assuming our ability to tune the adsorption properties of the adsorbent in any way desired, we can investigate the influence of various aspects of the adsorbent/isotherm. In the model, we described the adsorption isotherms by the dual-site Langmuir isotherm (Eq. 9).

$$n^{DSL} = \sum_{j=1}^{2} \frac{m_j \cdot b_{0,j} \cdot \exp\left(\frac{\Delta H_j}{R \cdot T}\right) \cdot P}{1 + b_{0,j} \cdot \exp\left(\frac{\Delta H_j}{R \cdot T}\right) \cdot P} \quad (9)$$

Where m_j is the saturation loading for site j, $b_{0,j}$ is the pre-exponential factor of the Langmuir constant for site j, ΔH_j is the enthalpy of adsorption for site j, and P is the partial pressure of the gas

species of interest. The dual-site Langmuir isotherm is based on two distinct, homogenous, adsorption sites.

View Article Online
DOI: 10.1039/C9ME00102F

First, we artificially increased the CO_2 capacity by multiplying *m* (Eq. 9) by a factor and we quantified the impact on the CO_2 purity, recovery and capture cost (Figure 6a-c). This exercise somewhat equals to increasing the selectivity of the adsorbent by increasing CO_2 capacity. In nearly every instance, increasing the CO_2 capacity of each adsorbent even by a factor of 20 has negligible impact. UTSA-16's CO_2 purity slightly improves up to a factor of 4, due to an increased working capacity. Beyond that, thermal effects offset the increase in CO_2 capacity. Improving the working capacity results in less adsorbent mass requirements and thereby a drop in cost. However, this effect remains small and restricted to low multiplication factor.

Next, we investigated the implications of reducing N_2 capacity (Figures 6d-f). This was achieved by dividing the corresponding *m* parameters in Eq. 9 by a factor. As before, this can be thought of improving the selectivity by reducing N_2 adsorption. This area has received little to no attention in the literature. We observe significant gains for the three outputs for the two MOFs, though the extent of improvement is less pronounced for UTSA-16. CO_2 purity improves due to a reduction in co-adsorption. The relative gain in CO_2 purity for UTSA-16 is not as large since the baseline sample does not adsorb significant amounts of N_2. Reducing N_2 adsorption improves CO_2 recovery for Mg-MOF-74. The N_2 working capacity on Mg-MOF-74 is rather high since Mg-MOF-74 adsorbs a significant amount of N_2 considering the partial pressure of N_2 for this application (Figure 2). In fact, the working capacity of N_2 is higher than CO_2, as indicated by the working selectivity values less than unity (Figure S9 to S12). The energetics of N_2 adsorption and desorption result in bed temperature swings. Reducing the portion of the temperature swing attributed to N_2 adsorption improves the CO_2 working capacity, and thus the recovery. This factor also enhances CO_2 purity. The improvements in recovery for Mg-MOF-74 culminate in significant capture cost reductions due to the smaller adsorbent mass required. For UTSA-16, CO_2 purity improves for the same reasons

View Article Online
DOI: 10.1039/C9ME00102F

mentioned above. The effect is not seen for CO_2 recovery due to significantly different N_2 adsorption characteristics of the baseline materials.

Finally, we assessed the effects of scaling the enthalpy of adsorption by varying ΔH (Eq. 9) for both CO_2 and N_2 by the same factor. We present the results in Figure 6g-i. For CO_2 purity, the maximum for Mg-MOF-74 is at ≈0.858×, and for UTSA-16 is at ≈1.01×. Taking the Δh^{ads} values referred to earlier, the optimum values become ≈40 kJ·mol^{-1} for CO_2 on Mg-MOF-74, and the baseline value of ≈32 – 35 kJ·mol^{-1} for UTSA-16. The overall trend in CO_2 purity as a function of enthalpy of adsorption is due to the trade-off between two scenarios. At lower ΔH, the isotherm is insufficiently steep to adsorb a useful amount at these low partial pressures, while at higher ΔH, the isotherm becomes too steep and working capacity suffers. The optimum value would therefore shift towards lower ΔH for higher feed concentrations with all other factors being equal. As the CO_2 recovery is a function of total feed amount, the influence of ΔH is multifaceted. A change in ΔH influences the amount adsorbed at a given partial pressure. Lower ΔH reduces the total amount adsorbed, thus the recovery is not impacted as dramatically as purity. At higher ΔH, the total amount adsorbed increases, while the amount that can be recovered decreases, resulting in a sharp decline in recovery. The minima in cost align with the maxima in recovery as a given mass of adsorbent is more productive, requiring less infrastructure. At lower ΔH, the capture cost increases due to poor working capacity attributed to the low amount adsorbed, requiring more adsorbent and vessels. At higher ΔH, poor working capacity arising from severe thermal effects increases cost.

Having assessed the effect of tuning various adsorbent properties, the question becomes: is this form of omnipotent control even possible? To some extent it may be. Increasing CO_2 adsorption capacity while operating in a physisorption regime would likely be attainable by increasing adsorbent surface area. The drawback to this is that N_2 adsorption capacity would correspondingly increase due to the non-selective nature of raw surface area. Selectively decreasing N_2 adsorption may be possible by reducing pore aperture, creating a molecular sieving style effect. Small pore MOFs with lower surface areas are uncommon and is an area which could benefit from additional research. Control

View Article Online
DOI: 10.1039/C9ME00102F

over the ΔH may be possible for both MOFs investigated here. Considering that the unsaturated metal sites of Mg-MOF-74 contribute most to the high adsorption enthalpy, two potential avenues arise. The first avenue is using other metal analogues of M-MOF-74 to modulate the M-CO_2 interactions and steric effects. This has been reported by Queen et al.[76] and based on this study, Co-, Fe-, Mn-, and Zn-MOF-74 may be more suitable than Mg-MOF-74. Partially metal substituted forms have also been developed[77], and such techniques may yield finer control. The second avenue is the grafting of organic molecules to the unsaturated metal sites[78–80]. The approach could be applied to control the enthalpy of adsorption by using mono or single-ended amines such as ethylamine for the most significant reduction, and functionalised forms such as aminoethanethiol, or ethanolamine for intermediate cases. An uncommon feature of UTSA-16 is the presence of charge-balancing cations (K^+) in the structure. A family of MOFs known as ZMOFs (zeolite like MOFs) also demonstrates this feature[81,82]. This feature could be exploited to influence the adsorbate-adsorbent interactions as is common in zeolites,[83–86] for instance *via* exchange with Li^+ ions.[87] Li^+ zeolites exhibit the strongest adsorbate-adsorbent interactions due to the high charge density of the Li^+ ion. A complete ion exchange would increase the heat of adsorption of UTSA-16. Whether this has the counter-effect of increasing the accessible pore size and N_2 adsorption remains to be seen. The authors also found that the Cs^+ form displayed the highest enthalpy of adsorption, which is contrary to the order displayed in zeolites. This area seems to warrant further investigation and rigorous gas adsorption studies.

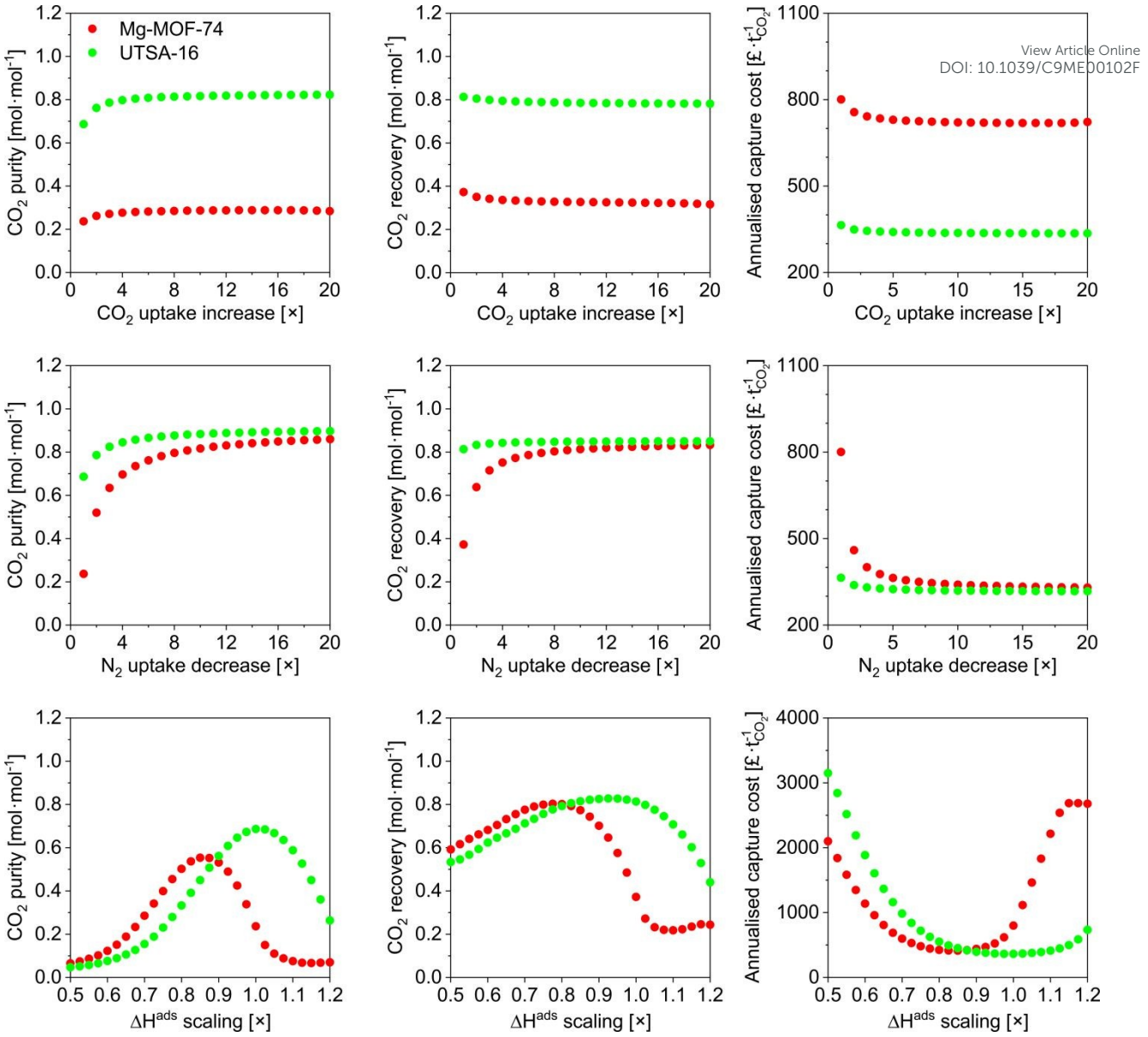

Figure 6. Influence of increasing CO_2 uptake (top), decreasing N_2 adsorption (middle), and enthalpy of adsorption (bottom) for Mg-MOF-74 (red) and UTSA-16 (green) on CO_2 purity (left), CO_2 recovery (middle), and capture cost (right) for the NGCC scenario.

The ideal isotherm

The previous section naturally leads to the question: what combination of CO_2 and N_2 isotherms are required to achieve maximum performance for the given scenarios? In response, we applied the model to generate a dataset by sweeping over a range of isotherm input parameters. Similar work has been previously undertaken[30,74], however, we assess a range of flue gas sources over a wider range

View Article Online
DOI: 10.1039/C9ME00102F

of isotherms, as well as considering capture cost. To reduce computation and data processing time, we used a single-site Langmuir isotherm (Eq. 10) in place of the dual-site Langmuir isotherm (Eq. 9), thereby reducing the number of isotherm input parameters from 12 to 6. To further reduce the number of input parameters, we made assumptions making use of the physical interpretation of the Langmuir isotherm model. Firstly, the saturation capacity, m, is made equal for both n_{CO2} and n_{N2} since the number of adsorption sites is constant for a given adsorbent. The parameter b_0 is related to the entropy of adsorption and assuming that the adsorbed phase is liquid-like allows the application of Trouton's rule[88], fixing the value of b_0 to $e^{-10.5}$ for both CO_2 and N_2. These assumptions allow the adsorption of CO_2 and N_2 to be described by three input parameters: m_{max}, ΔH_{CO2}, and ΔH_{N2}. Therefore, in effect, the amount adsorbed at a given pressure is defined by the value of ΔH. From the Langmuir isotherm theory, this is because a higher ΔH means a larger energy barrier must be overcome for the adsorbate to return to the gas phase. We swept the parameters over the following range, $1 \leq m_{max} \leq 16$ mol·kg^{-1}, $24 \leq \Delta H_{CO2} \leq 60$ kJ·mol^{-1}, and $11 \leq \Delta H_{N2} \leq 20$ kJ·mol^{-1}, in steps of 1, 2, and 1, respectively. We fixed the adsorbent physical properties throughout this process to the values of UTSA-16: bed density = 787 kg·m^{-3}, total void fraction = 0.61, and heat capacity = 878 J·kg^{-1}·K^{-1}. Including the variation of these parameters over a useful range would exponentially increase the number of data points and make data presentation unsightly. It may also be an unnecessary complication given the sensitivity analysis on physical properties discussed around Figure 3. The desorption pressure was fixed at 0.01 bar$_a$ for all cases.

$$n^{SSL} = \frac{m_{max} \cdot b_0 \cdot \exp\left(\frac{\Delta H}{R \cdot T}\right) \cdot P}{1 + b_0 \cdot \exp\left(\frac{\Delta H}{R \cdot T}\right) \cdot P} \quad (10)$$

Although the use of the single-site Langmuir isotherm means that some measured type-I adsorption isotherms cannot be fit very accurately, our aim is to uncover the relationship between the isotherm characteristics and process performance. For reference, the values of the three parameters for Mg-MOF-74 and UTSA-16 are provided in Table 2. Mg-MOF-74's CO_2 isotherms cannot be accurately

View Article Online
DOI: 10.1039/C9ME00102F

fit with the single-site model, however, the range between $0 \leq P \leq 0.40$ bar_a and $T \geq 303$ K displays good fitting performance. This is fortunate as it matches the range relevant to this work.

Table 2. Reduced single-site Langmuir isotherm fitting parameters for Mg-MOF-74 and UTSA-16.

Parameter	**Mg-MOF-74**	**UTSA-16**
$\mathbf{m_{max}}$ **[mol·kg^{-1}]**	7.54	4.16
$\mathbf{\Delta H_{CO2}}$ **[kJ·mol^{-1}]**	34.6	30.4
$\mathbf{\Delta H_{N2}}$ **[kJ·mol^{-1}]**	21.3	17.8

The outputs for CO_2 purity, recovery, and capture cost are shown in Figure 7 for all four scenarios. We first discuss CO_2 purity. The regions of good performance (red & grey) increase in size as the feed concentration increases indicating an easier separation. Taking the 11 kJ·mol^{-1} plane, the region defined by the yellow-green transition around ΔH_{CO2} of 48 kJ·mol^{-1} remains mostly unchanged when increasing CO_2 concentration. This represents the limitation imposed by thermal effects of the bed and regenerability. Even if the N_2 adsorption is negligible, a steep CO_2 isotherm will hamper performance. The regions in the lower left (low ΔH_{CO2}, high m_{max}) also increase in size with increasing CO_2 concentration. In the regions of low ΔH_{CO2}, a high capacity (m_{max}) is required in order to have an appreciable adsorption and working capacity at low feed concentrations. Hence, as the feed concentration increases, adsorbents with lower capacity also become feasible alternatives. For the 17 and 20 kJ·mol^{-1} planes, the good performance regions increase noticeably in size with feed CO_2 concentration. This increased allowance for N_2 adsorption from a pure-component isotherm perspective stems from the lower N_2 partial pressure in the feed. For the cement and steel scenarios, the dark blue-violet-black regions exhibit lower CO_2 purities than the feed concentration. This stems from high N_2 adsorption combined with poor CO_2 working capacity.

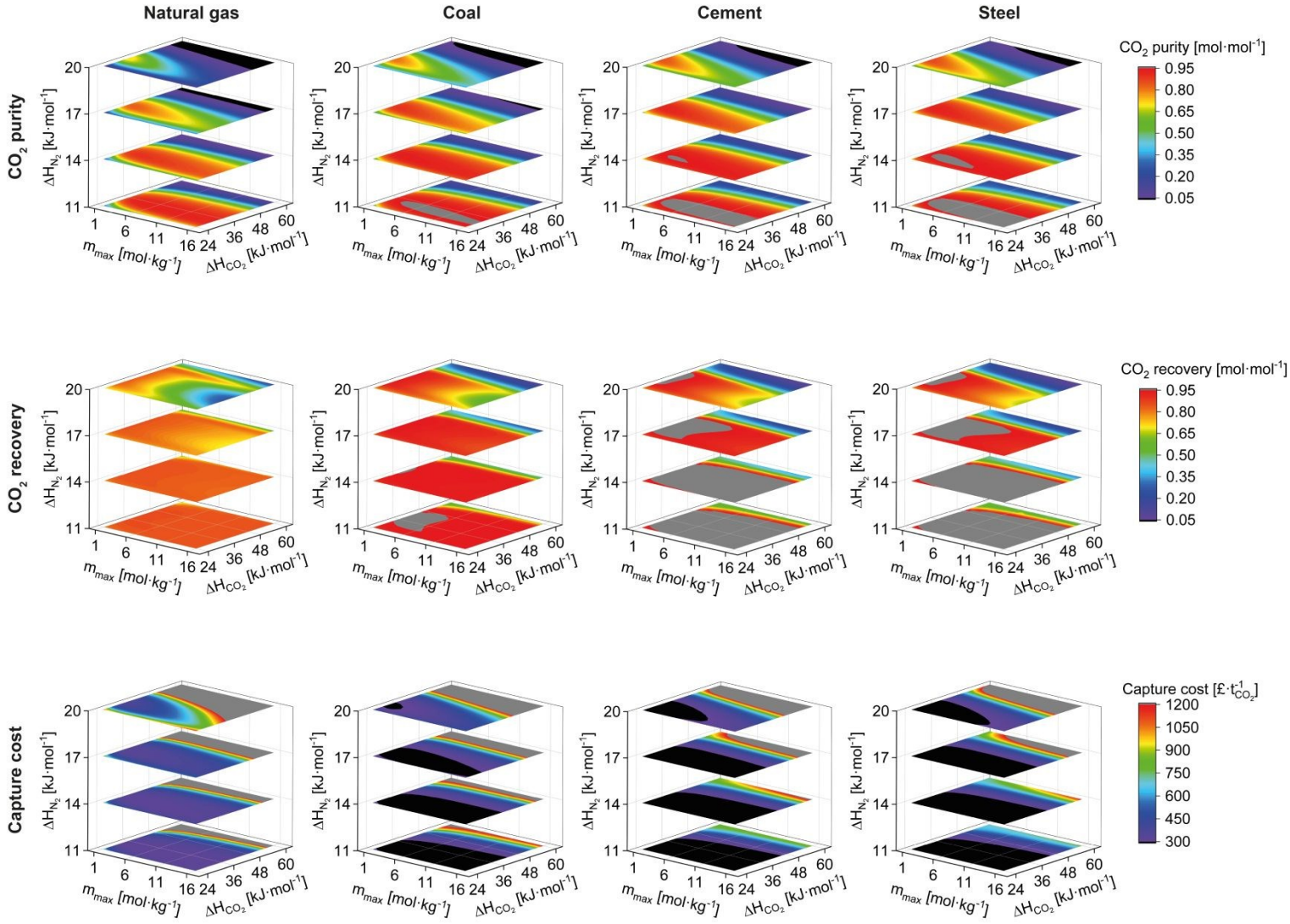

Figure 7. Contour plots displaying the influence of CO_2 and N_2 isotherm on CO_2 purity and recovery, and capture cost for the four post-combustion scenarios investigated. Only selected ΔH_{N2} layers are shown for greater clarity.

We now look at the variation in CO_2 recovery, *i.e.* the ratio between the CO_2 obtained in the product relative to the total CO_2 fed to the process. At the lower CO_2 concentrations, there are fewer regions of good recovery. Additionally, there is an appreciable amount of N_2 adsorption due to its comparatively high partial pressure. The ad- and desorption of CO_2 is not the sole contributor to the thermal effects of the bed, all species do. High, or increased, adsorption of N_2 leads to worse recovery of CO_2 as its desorption is hampering CO_2 desorption. This is reflected in two ways, any vertical line through the planes of ΔH_{N2} has reducing CO_2 recovery as N_2 adsorption increases, and a given ΔH_{N2} plane has reducing CO_2 recovery as m_{max} increases.

The capture cost contours highlight the areas of best CO_2 working capacity and recovery. Cross-scenario comparisons are not straightforward due to the differences in feed flow rate. The regions of lowest cost (black) increase in size with feed CO_2 concentration, somewhat expected due to the increasing ease of separation, driven mostly by improvements in CO_2 working capacity. If CO_2 working capacity did not have a significant effect, the regions of lowest cost would align with those of highest CO_2 recovery. In this model, as CO_2 purity is proportional to CO_2 working capacity, we observe similarities between the regions of lowest cost and highest purity (red & grey) for a given scenario.

We now return to our initial aim to define the ideal isotherm. In the framework of the single-site Langmuir isotherm, the parameter m_{max} would be proportional to the specific surface area (pore size and porosity), and the ΔH parameters to the respective adsorbate-adsorbent interactions (surface chemistry). It becomes possible to determine whether there is an isotherm type, and hence material properties, that are most suited for these separations. The utility of this exercise is to guide material development and enable a binary (yes/no) initial assessment of an adsorbent with minimal experimental input. Taking the natural gas scenario as an example, we generated a plot of all the isotherms achieving a CO_2 purity of 85 $\%_{mol}$ (Figure 8).

We observe no trend or commonality between the CO_2 isotherms that result in good process performance. Therefore, we cannot simply recommend a particular isotherm shape (and corresponding molecular scale properties), or CO_2 capacity, which yields good performance, further highlighting the limitations of using CO_2 adsorption capacity as a performance metric. It could be said in general that, given the N_2 loading of UTSA-16 at 273.15 K and 1 bar_a is 0.28 $mol \cdot kg^{-1}$, N_2 adsorption greater than this would render the adsorbent unsuitable for post-combustion capture using PVSA. For these styles of separations (*i.e.* post-combustion capture using adsorption), the co-adsorption of N_2 has the greatest influence on process performance. Consequently, efforts should be directed towards minimizing N_2 adsorption and this is in-line with previous work[30,74].

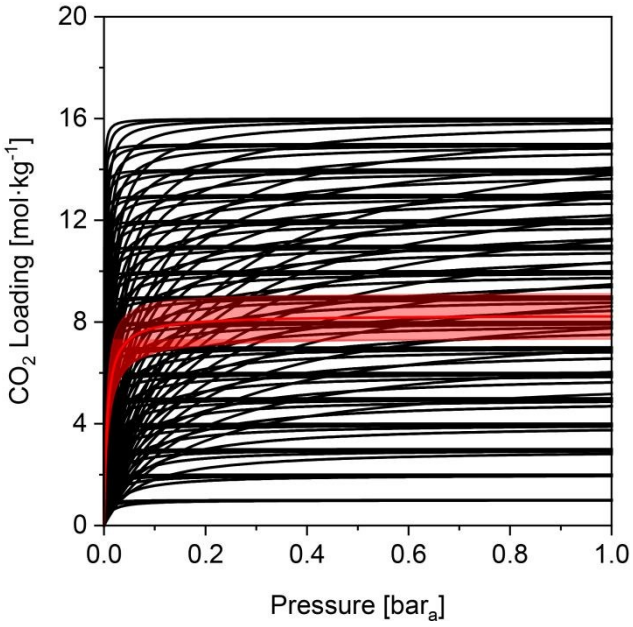

Figure 8. Representation of CO_2 isotherms that correspond to a CO_2 purity ≥ 85 $\%_{mol}$ for the NGCC scenario. The red line indicates the 'average' isotherm, with the shaded region showing the 99 % confidence interval. Calculated for 273.15 K.

Prima facie, for the NGCC scenario, one cannot achieve CO_2 purities $\geq 95\%_{mol}$ within the bounds investigated. However, the choice of adsorption cycle impacts the attainable purity for a given adsorbent, as discussed earlier. Zeolite 13X for the coal scenario at 0.01 bar_a desorption returned an $84\%_{mol}$ CO_2 purity. Separate studies showed that purities $\geq 95\%_{mol}$ and recoveries $\geq 90\%_{mol}$ are achievable using 13X[60,61]. Hence, using zeolite 13X as a reference, we hypothesise that isotherms with CO_2 purity values $\geq 85\%_{mol}$ could achieve the purity and recovery targets in a more complex cycle. The validity of this assumption depends on the concentration of CO_2 in the feed gas. At feed concentrations equal to or greater than for the coal combustion case ($12.5\%_{mol}$), there is little concern. At lower feed concentrations, it becomes more difficult to achieve the purity and recovery targets even with a more complex cycle. We could not locate experimental work or rigorous simulations for a PVSA process for post-combustion capture from natural gas. Therefore, we cannot quantitatively describe the uncertainty, or make an equivalent comparison for the natural gas scenario. In the absence of a sounder reference, we assume that adsorbents or isotherms which display CO_2 purity results $\geq 85\%_{mol}$ will achieve the required purity and recovery for CCS applications, albeit at a higher cost.

Establishing a surrogate model

Considering our previous analysis, we developed a surrogate model to simplify the evaluation of adsorbents. A surrogate model (*i.e.* black-box model) consists of one or more algebraic expressions fit to data, which enables regression of that data. The data generated in the previous section serves as the input, or training, data for the model. The data was fit using ALAMO[89]. ALAMO generates 'data-driven' surrogate models by combining multiple function types to fit the data using its solver, BARON. This surrogate model is meant to be used by researchers to quickly evaluate the performance of their adsorbents. We supply it here as

Supplementary Information. An example of the goodness-of-fit for the natural gas scenario is shown in Figure 9 by means of parity plots for three output variables. The complete results of the statistical analysis for all the scenarios are provided in the Supplementary Information (Figure S22 to S33). Given the robust goodness-of-fit of the surrogate model, we are confident that any adsorbent that is within the evaluated/swept bounds will be represented accurately.

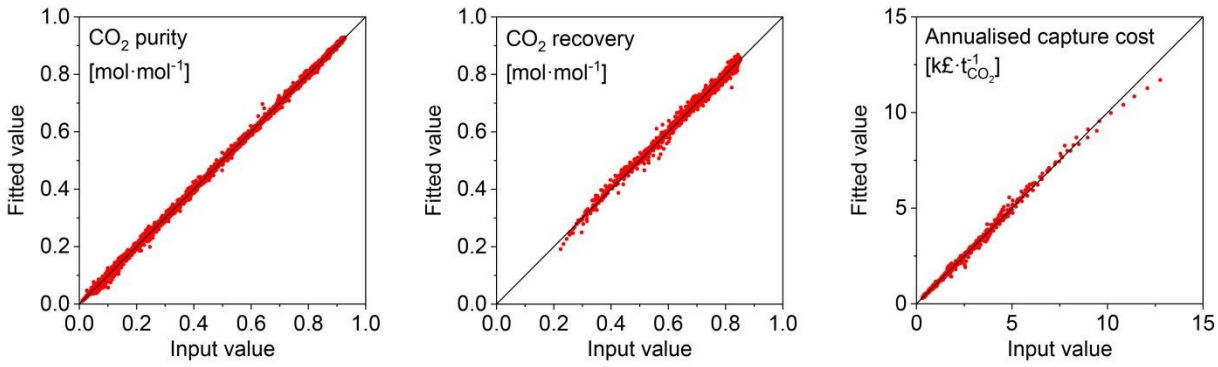

Figure 9. Parity plots of surrogate model fits for the natural-gas scenario data points to indicate the goodness-of-fit.

A surrogate model advantageously provides reasonable estimate of an adsorbent's performance, without the need to implement the complete model. To make use of the surrogate model, the user must measure CO_2 and N_2 isotherms at three temperatures and fit to the single-site Langmuir isotherm (Eq 10). We note that this equation may not perfectly fit the measured isotherm data (usually CO_2 data). However, as discussed earlier, as long as the data points in the pressure and temperature range of interest can be fit accurately, there are no ill-effects. While the number of isotherms needed may seem large, they are key to obtain a reliable evaluation of any adsorbent so the thermal effects can be elucidated. The other concern may be the adsorbent physical properties, as mentioned the data points are generated using the physical properties for UTSA-16. We addressed the implications of this assumption in the

sensitivity analysis (Figure 5). For an initial evaluation to gauge whether an adsorbent warrants detailed investigation, the repercussions are not severe.

CONCLUSIONS

We have screened 22 MOFs along with two zeolites and an activated carbon for CO_2/N_2 separation in four different CO_2 capture scenarios, *i.e*: NGCC, pulverised coal power plant, cement plant and integrated steel mill. The screening 'metrics' involved CO_2 purity, CO_2 recovery and capture cost (OPEX and CAPEX). Of the 22 MOFs evaluated, UTSA-16 performs the best. Its low N_2 uptake and less steep isotherms prevent product dilution by co-adsorbed N_2 and promote regenerability. UTSA-16's performance aligns with that of zeolite 13X. Mg-MOF-74 represents the worst choice of adsorbent for the targeted separation over all scenarios, due to its high adsorption enthalpy and high N_2 adsorption capacity. In our model, the performance displayed by UTSA remains below the targets in terms of purity and recovery, yet cycle optimisation would likely allow reaching these targets. Nonetheless, the process footprint requirements – at least 18,000 m^2 is required for the natural gas scenario – represent an area of concern, imposing limitations on, or discounts, retrofit possibilities. In addition, the cost of the separation remains generally high compared to the use of amine-based solvents. Interestingly, we have found that the cost of the adsorbent significant impacts that of the process only if it is above 50 £·kg^{-1}. A sensitivity analysis on adsorbent physical properties was also carried out to understand the impacts of uncertainty on these parameters. In general, uncertainties in heat capacity have the greatest influence on results, however, the magnitude is variable depending on the situation.

In the quest to identify optimum adsorbent characteristics that give best performance for CO_2 purity and recovery, and capture cost, we have 'optimised' UTSA-16 and Mg-MOF-74. Reducing N_2 adsorption has the greatest impact in increasing CO_2 purity and recovery, and

reducing capture cost. This should be a key area of research in materials development in the future. In addition, we have shown that an optimum heat of adsorption exists. Values cannot be too low such that the isotherm has little capacity at low CO_2 partial pressures such as those experienced in post-combustion capture, and it cannot be too high such that the working capacity and regenerability is hampered.

Finally, we have attempted to design an 'ideal adsorbent' by numerically screening all isotherms defined in a given range. Ultimately, it was not possible to define a single isotherm, or a group of similar isotherms, that meet the CO_2 purity and recovery requirements. However, we have used the data to develop a surrogate model and allow readers to swiftly evaluate their adsorbents for the four scenarios investigated without needing to implement the full model. This model requires users to input CO_2 and N_2 isotherms of their materials at 3 different temperatures each, in order to determine CO_2 purity and recovery.

The natural progression from here is to consider TSA given the technology advancements in the area, and the development of an associated model is underway to understand and evaluate TSA processes for post-combustion capture.

ACKNOWLEDGMENTS

We thank Mr. Wouter Arts for his efforts in surveying the literature for available isotherm data.

We are grateful to the EPSRC for providing the funding to undertake this research via the UK Carbon Capture and Storage Research Centre (UKCCSRC, grant EP/P026214/1).

ESI

View Article Online
DOI: 10.1039/C9ME00102F

Descriptions of the adsorption and absorption models, dual-site Langmuir isotherm parameters and physical properties of the adsorbents investigated, supplementary results, the digitised isotherm data, and a surrogate model for the readers' use, are supplied as Electronic Supplementary Information.

The following files are available:

Supplementary information (PDF)

Digitised isotherm data (XLSX)

Surrogate model (XLSX)

AUTHOR INFORMATION

Corresponding Authors

* Camille Petit

e-mail: camille.petit@imperial.ac.uk

Ph: +44 (0)20 7594 3182

* Niall Mac Dowell

e-mail: niall@imperial.ac.uk

Ph: +44 (0)20 7594 9298

ORCIDs

David Danaci – 0000-0002-7203-9655

Mai Bui – 0000-0002-2658-250X

Niall Mac Dowell – 0000-0002-0207-2900

Camille Petit – 0000-0002-3722-7984

View Article Online
DOI: 10.1039/C9ME00102F

REFERENCES

1 K. Sumida, S. Horike, S. S. Kaye, Z. R. Herm, W. L. Queen, C. M. Brown, F. Grandjean, G. J. Long, A. Dailly and J. R. Long, Hydrogen storage and carbon dioxide capture in an iron-based sodalite-type metal–organic framework (Fe-BTT) discovered via high-throughput methods, *Chem. Sci.*, 2010, **1**, 184.

2 P. Nugent, V. Rhodus, T. Pham, B. Tudor, K. Forrest, L. Wojtas, B. Space and M. Zaworotko, Enhancement of CO2 selectivity in a pillared pcu MOM platform through pillar substitution, *Chem. Commun.*, 2013, **49**, 1606.

3 Q.-Q. Dang, C.-Y. Liu, X.-M. Wang and X.-M. Zhang, Novel Covalent Triazine Framework for High-Performance CO2 Capture and Alkyne Carboxylation Reaction, *ACS Appl. Mater. Interfaces*, 2018, **10**, 27972–27978.

4 V. Guillerm, Ł. J. Weseliński, M. Alkordi, M. I. H. Mohideen, Y. Belmabkhout, A. J. Cairns and M. Eddaoudi, Porous organic polymers with anchored aldehydes: a new platform for post-synthetic amine functionalization en route for enhanced CO2 adsorption properties, *Chem. Commun.*, 2014, **50**, 1937.

5 W. Lu, D. Yuan, J. Sculley, D. Zhao, R. Krishna and H.-C. Zhou, Sulfonate-Grafted Porous Polymer Networks for Preferential CO2 Adsorption at Low Pressure, *J. Am. Chem. Soc.*, 2011, **133**, 18126–18129.

6 Y. Zeng, R. Zou and Y. Zhao, Covalent Organic Frameworks for CO2 Capture, *Adv. Mater.*, 2016, **28**, 2855–2873.

7 D.-H. Park, K. S. Lakhi, K. Ramadass, M.-K. Kim, S. N. Talapaneni, S. Joseph, U. Ravon, K. Al-Bahily and A. Vinu, Energy Efficient Synthesis of Ordered Mesoporous Carbon Nitrides with a High Nitrogen Content and Enhanced CO2 Capture Capacity, *Chem. - A Eur. J.*, 2017, **23**, 10753–10757.

8 A. Alabadi, S. Razzaque, Y. Yang, S. Chen and B. Tan, Highly porous activated carbon materials from carbonized biomass with high CO2 capturing capacity, *Chem. Eng. J.*, 2015, **281**, 606–612.

9 J. Chen, J. Yang, G. Hu, X. Hu, Z. Li, S. Shen, M. Radosz and M. Fan, Enhanced CO2 Capture Capacity of Nitrogen-Doped Biomass-Derived Porous Carbons, *ACS Sustain. Chem. Eng.*, 2016, **4**, 1439–1445.

10 R. Krishna and J. M. van Baten, A comparison of the CO2 capture characteristics of zeolites and metal–organic frameworks, *Sep. Purif. Technol.*, 2012, **87**, 120–126.

11 P. Harlick and F. Tezel, Equilibrium Analysis of Cyclic Adsorption Processes: CO2 Working Capacities with NaY, *Sep. Sci. Technol.*, 2005, **40**, 2569–2591.

12 D.-X. Xue, A. J. Cairns, Y. Belmabkhout, L. Wojtas, Y. Liu, M. H. Alkordi and M. Eddaoudi, Tunable Rare-Earth fcu-MOFs: A Platform for Systematic Enhancement of

CO2 Adsorption Energetics and Uptake, *J. Am. Chem. Soc.*, 2013, **135**, 7660–7667.

13 A. Phan, C. J. Doonan, F. J. Uribe-Romo, C. B. Knobler, M. O'Keeffe and O. M. Yaghi, Synthesis, Structure, and Carbon Dioxide Capture Properties of Zeolitic Imidazolate Frameworks, *Acc. Chem. Res.*, 2010, **43**, 58–67.

14 S. Salehi and M. Anbia, High CO2 Adsorption Capacity and CO2 /CH4 Selectivity by Nanocomposites of MOF-199, *Energy & Fuels*, 2017, **31**, 5376–5384.

15 A. Demessence, D. M. D'Alessandro, M. L. Foo and J. R. Long, Strong CO2 Binding in a Water-Stable, Triazolate-Bridged Metal−Organic Framework Functionalized with Ethylenediamine, *J. Am. Chem. Soc.*, 2009, **131**, 8784–8786.

16 J. Liu, P. K. Thallapally, B. P. McGrail, D. R. Brown and J. Liu, Progress in adsorption-based CO2 capture by metal–organic frameworks, *Chem. Soc. Rev.*, 2012, **41**, 2308–2322.

17 S. R. Caskey, A. G. Wong-Foy and A. J. Matzger, Dramatic Tuning of Carbon Dioxide Uptake via Metal Substitution in a Coordination Polymer with Cylindrical Pores, *J. Am. Chem. Soc.*, 2008, **130**, 10870–10871.

18 Z. Zhao, Z. Li and Y. S. Lin, Adsorption and Diffusion of Carbon Dioxide on Metal−Organic Framework (MOF-5), *Ind. Eng. Chem. Res.*, 2009, **48**, 10015–10020.

19 A. O. Yazaydın, R. Q. Snurr, T.-H. Park, K. Koh, J. Liu, M. D. LeVan, A. I. Benin, P. Jakubczak, M. Lanuza, D. B. Galloway, J. J. Low and R. R. Willis, Screening of Metal−Organic Frameworks for Carbon Dioxide Capture from Flue Gas Using a Combined Experimental and Modeling Approach, *J. Am. Chem. Soc.*, 2009, **131**, 18198–18199.

20 E. S. Kikkinides, R. T. Yang and S. H. Cho, Concentration and recovery of carbon dioxide from flue gas by pressure swing adsorption, *Ind. Eng. Chem. Res.*, 1993, **32**, 2714–2720.

21 K. T. Chue, J. N. Kim, Y. J. Yoo, S. H. Cho and R. T. Yang, Comparison of Activated Carbon and Zeolite 13X for CO2 Recovery from Flue Gas by Pressure Swing Adsorption, *Ind. Eng. Chem. Res.*, 1995, **34**, 591–598.

22 W.-K. Choi, T.-I. Kwon, Y.-K. Yeo, H. Lee, H. K. Song and B.-K. Na, Optimal operation of the pressure swing adsorption (PSA) process for CO2 recovery, *Korean J. Chem. Eng.*, 2003, **20**, 617–623.

23 S. P. Reynolds, A. D. Ebner and J. A. Ritter, Stripping PSA Cycles for CO2 Recovery from Flue Gas at High Temperature Using a Hydrotalcite-Like Adsorbent, *Ind. Eng. Chem. Res.*, 2006, **45**, 4278–4294.

24 P. Xiao, J. Zhang, P. Webley, G. Li, R. Singh and R. Todd, Capture of CO2 from flue gas streams with zeolite 13X by vacuum-pressure swing adsorption, *Adsorption*, 2008,

View Article Online
DOI: 10.1039/C9ME00102F

14, 575–582.

25 J. A. Delgado, M. A. Uguina, J. L. Sotelo, V. I. Águeda, A. Sanz and P. Gómez, Numerical analysis of CO2 concentration and recovery from flue gas by a novel vacuum swing adsorption cycle, *Comput. Chem. Eng.*, 2011, **35**, 1010–1019.

26 Z. Liu, C. A. Grande, P. Li, J. Yu and A. E. Rodrigues, Multi-bed Vacuum Pressure Swing Adsorption for carbon dioxide capture from flue gas, *Sep. Purif. Technol.*, 2011, **81**, 307–317.

27 R. Haghpanah, A. Majumder, R. Nilam, A. Rajendran, S. Farooq, I. A. Karimi and M. Amanullah, Multiobjective Optimization of a Four-Step Adsorption Process for Postcombustion CO2 Capture Via Finite Volume Simulation, *Ind. Eng. Chem. Res.*, 2013, **52**, 4249–4265.

28 Y. Shen, Y. Zhou, D. Li, Q. Fu, D. Zhang and P. Na, Dual-reflux pressure swing adsorption process for carbon dioxide capture from dry flue gas, *Int. J. Greenh. Gas Control*, 2017, **65**, 55–64.

29 G. N. Nikolaidis, E. S. Kikkinides and M. C. Georgiadis, An Integrated Two-Stage P/VSA Process for Postcombustion CO2 Capture Using Combinations of Adsorbents Zeolite 13X and Mg-MOF-74, *Ind. Eng. Chem. Res.*, 2017, **56**, 974–988.

30 B. J. Maring and P. A. Webley, A new simplified pressure/vacuum swing adsorption model for rapid adsorbent screening for CO2 capture applications, *Int. J. Greenh. Gas Control*, 2013, **15**, 16–31.

31 G. D. Pirngruber, L. Hamon, S. Bourrelly, P. L. Llewellyn, E. Lenoir, V. Guillerm, C. Serre and T. Devic, A Method for Screening the Potential of MOFs as CO2 Adsorbents in Pressure Swing Adsorption Processes, *ChemSusChem*, 2012, **5**, 762–776.

32 L. Joss, M. Gazzani, M. Hefti, D. Marx and M. Mazzotti, Temperature Swing Adsorption for the Recovery of the Heavy Component: An Equilibrium-Based Shortcut Model, *Ind. Eng. Chem. Res.*, 2015, **54**, 3027–3038.

33 M. Hefti, L. Joss, Z. Bjelobrk and M. Mazzotti, On the potential of phase-change adsorbents for CO2 capture by temperature swing adsorption, *Faraday Discuss.*, 2016, **192**, 153–179.

34 V. Subramanian Balashankar, A. K. Rajagopalan, R. de Pauw, A. M. Avila and A. Rajendran, Analysis of a Batch Adsorber Analogue for Rapid Screening of Adsorbents for Postcombustion CO2 Capture, *Ind. Eng. Chem. Res.*, 2019, **58**, 3314–3328.

35 P. A. Webley, A. Qader, A. Ntiamoah, J. Ling, P. Xiao and Y. Zhai, A New Multi-bed Vacuum Swing Adsorption Cycle for CO2 Capture from Flue Gas Streams, *Energy Procedia*, 2017, **114**, 2467–2480.

36 H. Wu, W. Zhou and T. Yildirim, High-capacity methane storage in metal-organic

frameworks M2(dhtp): the important role of open metal sites., *J. Am. Chem. Soc.*, 2009, **131**, 4995–5000.

37 J. R. Rumble, Ed., in *CRC Handbook of Chemistry and Physics, 100th Edition (Internet Version 2019)*, CRC Press/Taylor & Francis, Boca Raton, FL, 2019.

38 B. T. Goodman, W. V. Wilding, J. L. Oscarson and R. L. Rowley, Use of the DIPPR Database for Development of Quantitative Structure−Property Relationship Correlations: Heat Capacity of Solid Organic Compounds †, *J. Chem. Eng. Data*, 2004, **49**, 24–31.

39 J. Park, J. D. Howe and D. S. Sholl, How Reproducible Are Isotherm Measurements in Metal–Organic Frameworks?, *Chem. Mater.*, 2017, **29**, 10487–10495.

40 R. Han, K. S. Walton and D. S. Sholl, Does Chemical Engineering Research Have a Reproducibility Problem?, *Annu. Rev. Chem. Biomol. Eng.*, 2019, **10**, 43–57.

41 S. Mohammad, J. Fitzgerald, R. L. Robinson and K. A. M. Gasem, Experimental Uncertainties in Volumetric Methods for Measuring Equilibrium Adsorption, *Energy & Fuels*, 2009, **23**, 2810–2820.

42 Y. Gensterblum, P. van Hemert, P. Billemont, A. Busch, D. Charriére, D. Li, B. M. Krooss, G. de Weireld, D. Prinz and K.-H. A. A. Wolf, European inter-laboratory comparison of high pressure CO2 sorption isotherms. I: Activated carbon, *Carbon N. Y.*, 2009, **47**, 2958–2969.

43 Y. Gensterblum, P. van Hemert, P. Billemont, E. Battistutta, A. Busch, B. M. Krooss, G. De Weireld and K.-H. A. A. Wolf, European inter-laboratory comparison of high pressure CO2 sorption isotherms II: Natural coals, *Int. J. Coal Geol.*, 2010, **84**, 115–124.

44 IEA Greenhouse Gas R&D Programme (IEA GHG), *CO2 Capture in the Cement Industry*, 2008.

45 IEA Greenhouse Gas R&D Programme (IEA GHG), *Iron and Steel CCS Study (Techno-Economics Integrated Steel Mill)*, 2013.

46 D. J. Brennan, *Process Industry Economics: An International Perspective*, IChemE, Rugby, UK, 1997.

47 D. J. Brennan and K. A. Golonka, New Factors for Capital Cost Estimation in Evolving Process Designs, *Chem. Eng. Res. Des.*, 2002, **80**, 579–586.

48 P.-E. Just, Advances in the development of CO2 capture solvents, *Energy Procedia*, 2013, **37**, 314–324.

49 M. T. Ho, G. W. Allinson and D. E. Wiley, Reducing the Cost of CO2 Capture from Flue Gases Using Pressure Swing Adsorption, *Ind. Eng. Chem. Res.*, 2008, **47**, 4883–

View Article Online
DOI: 10.1039/C9ME00102F

4890.

50 N. Susarla, R. Haghpanah, I. A. Karimi, S. Farooq, A. Rajendran, L. S. C. Tan and J. S. T. Lim, Energy and cost estimates for capturing CO2 from a dry flue gas using pressure/vacuum swing adsorption, *Chem. Eng. Res. Des.*, 2015, **102**, 354–367.

51 D. E. Garrett, *Chemical Engineering Economics*, van Nostrand Reinhold, New York, 1989.

52 M. R. M. Abu-Zahra, J. P. M. Niederer, P. H. M. Feron and G. F. Versteeg, CO2 capture from power plants, *Int. J. Greenh. Gas Control*, 2007, **1**, 135–142.

53 A. Raksajati, M. T. Ho and D. E. Wiley, Reducing the Cost of CO2 Capture from Flue Gases Using Aqueous Chemical Absorption, *Ind. Eng. Chem. Res.*, 2013, **52**, 16887–16901.

54 M. Vaccarelli, R. Carapellucci and L. Giordano, Energy and Economic Analysis of the CO2 Capture from Flue Gas of Combined Cycle Power Plants, *Energy Procedia*, 2014, **45**, 1165–1174.

55 G. Manzolini, E. Sanchez Fernandez, S. Rezvani, E. Macchi, E. L. V. Goetheer and T. J. H. Vlugt, Economic assessment of novel amine based CO2 capture technologies integrated in power plants based on European Benchmarking Task Force methodology, *Appl. Energy*, 2015, **138**, 546–558.

56 K. Li, W. Leigh, P. Feron, H. Yu and M. Tade, Systematic study of aqueous monoethanolamine (MEA)-based CO2 capture process: Techno-economic assessment of the MEA process and its improvements, *Appl. Energy*, 2016, **165**, 648–659.

57 G. Guandalini, M. C. Romano, M. Ho, D. Wiley, E. S. Rubin and J. C. Abanades, A sequential approach for the economic evaluation of new CO2 capture technologies for power plants, *Int. J. Greenh. Gas Control*, 2019, **84**, 219–231.

58 J. A. Mason, K. Sumida, Z. R. Herm, R. Krishna and J. R. Long, Evaluating metal–organic frameworks for post-combustion carbon dioxide capture via temperature swing adsorption, *Energy Environ. Sci.*, 2011, **4**, 3030.

59 Z. Zhang, S. Xian, Q. Xia, H. Wang, Z. Li and J. Li, Enhancement of CO2 Adsorption and CO2/N2 Selectivity on ZIF-8 via Postsynthetic Modification, *AIChE J.*, 2013, **59**, 2195–2206.

60 R. Haghpanah, R. Nilam, A. Rajendran, S. Farooq and I. A. Karimi, Cycle synthesis and optimization of a VSA process for postcombustion CO2 capture, *AIChE J.*, 2013, **59**, 4735–4748.

61 D. Diagne, M. Goto and T. Hirose, Parametric Studies on CO2 Separation and Recovery by a Dual Reflux PSA Process Consisting of Both Rectifying and Stripping Sections, *Ind. Eng. Chem. Res.*, 1995, **34**, 3083–3089.

62 A. Agarwal, L. T. Biegler and S. E. Zitney, A superstructure-based optimal synthesis of PSA cycles for post-combustion CO2 capture, *AIChE J.*, 2009, **56**, 1813–1828.

63 G. T. Rochelle, in *Absorption-Based Post-combustion Capture of Carbon Dioxide*, Elsevier, 2016, pp. 35–67.

64 E. S. Rubin, S. Yeh, M. Antes, M. Berkenpas and J. Davison, Use of experience curves to estimate the future cost of power plants with CO2 capture, *Int. J. Greenh. Gas Control*, 2007, **1**, 188–197.

65 M. M. F. Hasan, E. L. First, F. Boukouvala and C. A. Floudas, A multi-scale framework for CO2 capture, utilization, and sequestration: CCUS and CCU, *Comput. Chem. Eng.*, 2015, **81**, 2–21.

66 C. Kolster, E. Mechleri, S. Krevor and N. Mac Dowell, The role of CO2 purification and transport networks in carbon capture and storage cost reduction, *Int. J. Greenh. Gas Control*, 2017, **58**, 127–141.

67 A. Masala, J. G. Vitillo, G. Mondino, C. A. Grande, R. Blom, M. Manzoli, M. Marshall and S. Bordiga, CO2 Capture in Dry and Wet Conditions in UTSA-16 Metal–Organic Framework, *ACS Appl. Mater. Interfaces*, 2017, **9**, 455–463.

68 V. K. Chuikina, A. V. Kiselev, L. V. Mineyeva and G. G. Muttik, Heats of adsorption of water vapour on NaX and KNaX zeolites at different temperatures, *J. Chem. Soc. Faraday Trans. 1 Phys. Chem. Condens. Phases*, 1976, **72**, 1345.

69 K. N. Son, T.-M. J. Richardson and G. E. Cmarik, Equilibrium Adsorption Isotherms for H2O on Zeolite 13X, *J. Chem. Eng. Data*, 2019, **64**, 1063–1071.

70 Inventys Inc., Technology, http://inventysinc.com/technology/, (accessed 14 July 2019).

71 US Department of Energy, MOVE Program Overview, https://arpa-e.energy.gov/sites/default/files/documents/files/MOVE_ProgramOverview.pdf, (accessed 28 July 2019).

72 Z. Bao, L. Yu, Q. Ren, X. Lu and S. Deng, Adsorption of CO2 and CH4 on a magnesium-based metal organic framework, *J. Colloid Interface Sci.*, 2011, **353**, 549–556.

73 A. Masala, F. Grifasi, C. Atzori, J. G. Vitillo, L. Mino, F. Bonino, M. R. Chierotti and S. Bordiga, CO2 Adsorption Sites in UTSA-16: Multitechnique Approach, *J. Phys. Chem. C*, 2016, **120**, 12068–12074.

74 A. K. Rajagopalan and A. Rajendran, The effect of nitrogen adsorption on vacuum swing adsorption based post-combustion CO2 capture, *Int. J. Greenh. Gas Control*, 2018, **78**, 437–447.

75 R. Zhao, S. Deng, S. Wang, L. Zhao, Y. Zhang, B. Liu, H. Li and Z. Yu, Thermodynamic

research of adsorbent materials on energy efficiency of vacuum-pressure swing adsorption cycle for CO2 capture, *Appl. Therm. Eng.*, 2018, **128**, 818–829.

76 W. L. Queen, M. R. Hudson, E. D. Bloch, J. A. Mason, M. I. Gonzalez, J. S. Lee, D. Gygi, J. D. Howe, K. Lee, T. A. Darwish, M. James, V. K. Peterson, S. J. Teat, B. Smit, J. B. Neaton, J. R. Long and C. M. Brown, Comprehensive study of carbon dioxide adsorption in the metal–organic frameworks M2(dobdc) (M = Mg, Mn, Fe, Co, Ni, Cu, Zn), *Chem. Sci.*, 2014, **5**, 4569–4581.

77 Y. Jiao, C. R. Morelock, N. C. Burtch, W. P. Mounfield, J. T. Hungerford and K. S. Walton, Tuning the Kinetic Water Stability and Adsorption Interactions of Mg-MOF-74 by Partial Substitution with Co or Ni, *Ind. Eng. Chem. Res.*, 2015, **54**, 12408–12414.

78 S. Choi, T. Watanabe, T.-H. Bae, D. S. Sholl and C. W. Jones, Modification of the Mg/DOBDC MOF with Amines to Enhance CO2 Adsorption from Ultradilute Gases, *J. Phys. Chem. Lett.*, 2012, **3**, 1136–1141.

79 X. Su, L. Bromberg, V. Martis, F. Simeon, A. Huq and T. A. Hatton, Postsynthetic Functionalization of Mg-MOF-74 with Tetraethylenepentamine: Structural Characterization and Enhanced CO 2 Adsorption, *ACS Appl. Mater. Interfaces*, 2017, **9**, 11299–11306.

80 T. M. McDonald, W. R. Lee, J. A. Mason, B. M. Wiers, C. S. Hong and J. R. Long, Capture of Carbon Dioxide from Air and Flue Gas in the Alkylamine-Appended Metal–Organic Framework mmen-Mg2(dobpdc), *J. Am. Chem. Soc.*, 2012, **134**, 7056–7065.

81 F. Nouar, J. Eckert, J. F. Eubank, P. Forster and M. Eddaoudi, Zeolite- like Metal−Organic Frameworks (ZMOFs) as Hydrogen Storage Platform: Lithium and Magnesium Ion-Exchange and H2-(rho-ZMOF) Interaction Studies, *J. Am. Chem. Soc.*, 2009, **131**, 2864–2870.

82 G. Calleja, J. A. Botas, M. Sánchez-Sánchez and M. G. Orcajo, Hydrogen adsorption over Zeolite-like MOF materials modified by ion exchange, *Int. J. Hydrogen Energy*, 2010, **35**, 9916–9923.

83 D. W. Breck, *Zeolite Molecular Sieves: Structure, Chemistry and Use*, John Wiley & Sons, Inc., New York, 1974.

84 R. M. Barrer and R. M. Gibbons, Zeolitic carbon dioxide: energetics and equilibria in relation to exchangeable cations in faujasite, *Trans. Faraday Soc.*, 1965, **61**, 948.

85 J. Zhang, R. Singh and P. A. Webley, Alkali and alkaline-earth cation exchanged chabazite zeolites for adsorption based CO2 capture, *Microporous Mesoporous Mater.*, 2008, **111**, 478–487.

86 K. S. Walton, M. B. Abney and M. Douglas LeVan, CO2 adsorption in Y and X zeolites modified by alkali metal cation exchange, *Microporous Mesoporous Mater.*, 2006, **91**, 78–84.

87 X. Zhang, Z. Chen, X. Yang, M. Li, C. Chen and N. Zhang, The fixation of carbon dioxide with epoxides catalyzed by cation-exchanged metal-organic framework, *Microporous Mesoporous Mater.*, 2018, **258**, 55–61.

88 A. L. Myers and F. Siperstein, Characterization of adsorbents by energy profile of adsorbed molecules, *Colloids Surfaces A Physicochem. Eng. Asp.*, 2001, **187–188**, 73–81.

89 Z. T. Wilson and N. V. Sahinidis, The ALAMO approach to machine learning, *Comput. Chem. Eng.*, 2017, **106**, 785–795.